Journal of Medicinal Chemistry

Article

5-(4,6-Dimorpholino-1,3,5-triazin-2-yl)-4-(trifluoromethyl)pyridin-2-amine (PQR309): a Potent, Brain-Penetrant, Orally Bioavailable, pan-Class I PI3K/mTOR Inhibitor as Clinical Candidate in Oncology

Florent Beaufils, Natasa Cmiljanovic, Vladimir Cmiljanovic, Thomas Bohnacker, Anna Melone, Romina Marone, Eileen Jackson, Xuxiao Zhang, Alexander Sele, Chiara Borsari, Jürgen Mestan, Paul Hebeisen, Petra Hillmann, Bernd Giese, Marketa Zvelebil, Doriano Fabbro, Roger L. Williams, Denise Rageot, and Matthias P. Wymann

J. Med. Chem., **Just Accepted Manuscript** • DOI: 10.1021/acs.jmedchem.7b00930 • Publication Date (Web): 22 Aug 2017

Just Accepted

ACS Publications

Journal of Medicinal Chemistry is published by the American Chemical Society. 1155 Sixteenth Street N.W., Washington, DC 20036

5-(4,6-Dimorpholino-1,3,5-triazin-2-yl)-4-(trifluoromethyl)pyridin-2-amine (PQR309): a Potent, Brain-Penetrant, Orally Bioavailable, pan-Class I PI3K/mTOR Inhibitor as Clinical Candidate in Oncology

Florent Beaufils[1,†,$], Natasa Cmiljanovic[1,†,$], Vladimir Cmiljanovic[1,†,$], Thomas Bohnacker[1], Anna Melone[1], Romina Marone[1], Eileen Jackson[1], Xuxiao Zhang[2], Alexander Sele[1], Chiara Borsari[1], Jürgen Mestan[3], Paul Hebeisen[3], Petra Hillmann[3], Bernd Giese[4,††], Marketa Zvelebil[1], Doriano Fabbro[3], Roger L. Williams[2], Denise Rageot[1,*], Matthias P. Wymann[1,*]

[1]Department of Biomedicine, University of Basel, Mattenstrasse 28, 4058 Basel, Switzerland;

[2]MRC Laboratory of Molecular Biology, Francis Crick Avenue, Cambridge CB2 0QH, UK;

[3]PIQUR Therapeutics AG, Hochbergerstrasse 60C, 4057 Basel, Switzerland;

[4]Department of Chemistry, University of Basel, St. Johanns-Ring 19, 4056 Basel, Switzerland.

Current address:

[†]PIQUR Therapeutics AG, Basel, Switzerland;

[††]Department of Chemistry, University of Fribourg, Fribourg, Switzerland.

[$]These authors contributed equally to this work.

*Correspondence to:

Matthias.Wymann@UniBas.CH and Denise.Rageot@UniBas.CH

Dept. Biomedicine, University of Basel

Mattenstrasse 28

4058 Basel, Switzerland

Tel. +41 61 207 5046; Fax. +41 61 207 3566

ABSTRACT

Phosphoinositide-3-kinase (PI3K) is deregulated in a wide variety of human tumors, and triggers activation of protein kinase B (PKB/Akt) and mammalian target of rapamycin (mTOR). Here we describe the preclinical characterization of compound **1** (PQR309, Bimiralisib), a potent 4,6-dimorpholino-1,3,5-triazine-based pan-class I PI3K inhibitor, which targets mTOR kinase in a balanced fashion at higher concentrations. No off-target interactions were detected for **1** in a wide panel of protein kinase, enzyme, and receptor ligand assays. Moreover, **1** did not bind tubulin, which was observed for the structurally related **4** (BKM120, Buparlisib). Compound **1** is orally available, crosses the blood-brain barrier, and displayed favorable pharmacokinetic parameters in mice, rats, and dogs. Compound **1** demonstrated efficiency inhibiting proliferation in tumor cell lines, and a rat xenograft model. This, together with the compound's safety profile identifies **1** as a clinical candidate with a broad application range in oncology, including treatment of brain tumors or CNS metastasis. Compound **1** is currently in phase II clinical trials for advanced solid tumors and refractory lymphoma.

INTRODUCTION

Phosphoinositide 3-kinases (PI3Ks) are lipid kinases that play a central role in the control of cancer cell growth, proliferation and metastasis.[1–3] The PI3K family is divided into three classes according to sequence homology and substrate specificity: so-called class I PI3Ks are activated downstream of cell surface receptors, including receptor protein tyrosine kinases (RTKs), immunoglobulin receptors and G-protein coupled receptors (GPCRs). Class IA PI3Ks consist of the catalytic subunits p110α, p110β, and p110δ. These interact with dedicated phosphorylated tyrosine motifs on growth factor receptors or their substrates via two src-homology 2 (SH2) domains present in their tightly associated p85 regulatory subunits. The class IB PI3Kγ operates downstream of GPCRs, and is composed of a catalytic subunit p110γ and an adapter subunit, which is either p84 or p101.[4]

Class I PI3Ks phosphorylate phosphatidylinositol(4,5)-bisphosphate [PtdIns(4,5)P_2] to yield phosphatidylinositol(3,4,5)-trisphosphate [PtdIns(3,4,5)P_3]. PtdIns(3,4,5)P_3, produced at the inner leaflet of the plasma membrane, provides a docking site for effector proteins with Pleckstrin-homology (PH) domains. The serine/threonine kinases phosphoinositide-dependent kinase 1 (PDK-1) and protein kinase B (PKB/Akt) contain a PH domain, and are thus activated by PI3K, and relay the activation of the mammalian target of rapamycin complex 1 (mTORC1). In tumor cells, hyper-activation of the PI3K/mTOR pathway can occur on multiple levels, including mutation or overexpression of cell surface receptors such as HER2[5], oncogenes, the protein tyrosine phosphatase non-receptor 12 (PTPN12)[6], or the presence of activating hotspot mutations in PIK3CA (encoding the catalytic PI3Kα subunit p110α).[7] Other key regulators of the PI3K pathway include the lipid phosphatase PTEN hydrolyzing PtdIns(3,4,5)P_3 back to PtdIns(4,5)P_2,[2,8] and the inositol polyphosphate 4-phosphatase type II (INPP4B)[9] degrading PtdIns(3,4)P_2. Loss of either lipid phosphatase activities or gain of function mutations at the level of PI3K, and aberrations up- and downstream in the pathway can thus lead to the constitutive activation of PI3K, PKB/Akt and mTOR.

Besides promotion of tumor cell growth and angiogenesis, an over-activated PI3K/mTOR pathway has been associated with resistance to other cancer treatments, *e.g.* receptor tyrosine kinase inhibitors. PI3K inactivating agents are currently in various clinical trials as either monotherapy or in combination with other drugs.[2,3,10]

In our search for the development of a dual pan-PI3K/mTOR inhibitor, we focused on di-morpholino substituted compounds with a triazine core, as their symmetry supports rapid access to a compound library with

various aryl substituents. Furthermore, our goal was to develop brain-penetrable compounds, to allow for the treatment of brain metastasis and brain tumors. Here we describe a SAR study around the aryl moiety at the C2-position of bismorpholino-triazines, which led to the identification of **1** (PQR309, Bimiralisib)[11], a clinical candidate and brain penetrable pan-PI3K/mTOR inhibitor.

RESULTS AND DISCUSSION

Compound **1** evolved as the lead compound of a series of dimorpholino-triazine based compounds, and is currently tested in Phase II clinical trials (clinicaltrials.gov). Initially inspired by 2-(2-difluoromethylbenzimidazol-1-yl)-4,6-dimorpholino-1,3,5-triazine (ZSTK474)[12], a pan PI3K inhibitor with a triazine core, development of **1** aimed to *i*) maximize compound solubility and bioavailability, ii) achieve blood brain barrier penetration, iii) avoid microtubule interactions as observed for **4** (BKM120, Buparlisib)[11,13], and *iv*) introduce moderate mTOR inhibition. The rational for PI3K/mTOR dual activity was based on the observation that persistent mTOR signaling was reported to confer resistance to PI3K inhibition[14], while selective targeting of the mTOR complex 1 (TORC1) initiates positive feedback leading to PI3K hyper-activation[15]. To avoid this, we selected for compounds with a higher potency for PI3K than mTOR kinase. Moreover, drugs targeting both PI3K and mTOR have been shown early on to be more effective in tumors with multiple pathway activation such as melanoma[16,17], and to potentially support drug combinations[18].

A number of clinically advanced PI3K inhibitors with a pyrimidine, triazine or fused pyrimidine core contain at least one morpholine moiety. This morpholine was demonstrated to be a crucial feature for PI3K binding, as the morpholine oxygen atom forms a hydrogen bond interaction with the hinge region backbone NH of the amino acid residue Val851 in PI3Kα (Val882 in PI3Kγ, and Val2240 in mTOR). Structurally related compounds, which display distinct PI3K and mTOR kinase inhibitory profiles (Table 1) are shown in Figure 1: **1**, **4**[19] and **6** (GDC-0980, Apitolisib / RG7422)[20] target PI3K and mTOR kinase with some preference for PI3Kα, while **3** (PIK-587, Gedatolisib/ PF-05212384)[21] is a potent dual PI3K/mTOR inhibitor, and **5** (GDC-0941, Pictilisib)[22] targets PI3K.

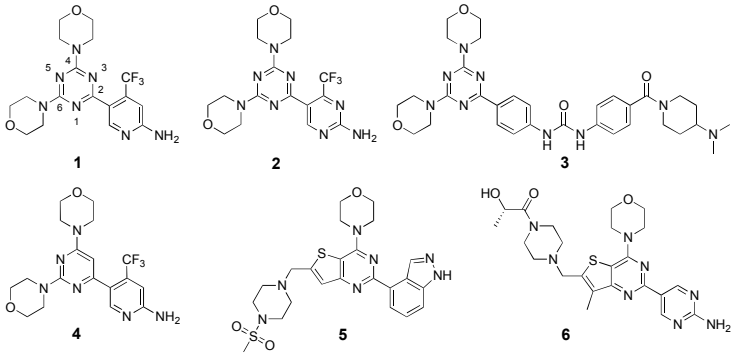

Figure 1. Structure of triazine core PI3K inhibitors **1**, reference compound **2**, and reported clinical candidate **3**; and pyrimidine or fused pyrimidine core containing molecules **4**, **5**, and **6**.

The above compounds are substituted with various aryl moieties (*e.g.* indazole, pyrimidine, pyridine, benzoimidazole or aniline), which are situated in the PI3K's ATP-binding site towards the affinity binding pocket. The primary amine of **4**[11,19] and **6**,[20] interacts *via* hydrogen bonding with the carboxyl groups of the amino acid residues Asp841 and Asp836 in PI3Kγ. For **3** it has been proposed that the urea-NH groups form hydrogen bonds with Asp810 and the urea oxygen engages the wortmannin-reactive Lys802[23,24] in PI3Kα.[25] Finally, **5** exploits its indazole N-NH atoms to form hydrogen bonds with Tyr867 and Asp841 in PI3Kγ. As illustrated by the exchange of the aryl moiety from 4-(trifluoromethyl)pyridin-2-amine in **1** to 4-(trifluoromethyl)pyrimidin-2-amine in compound **2**, the aryl substitution can be used to fine tune PI3K vs. mTOR activity.

Table 1. Affinity of triazine and pyrimidine core-containing molecules to PI3K and PI3K-related Kinases

	Binding constants K_d, [nM][a]									**mTOR/ PI3Kα**
Kinase→	PI3Kα	PI3Kβ	PI3Kγ	PI3Kδ	mTOR	PI3KC2β	VPS34	PI4KCβ	DNAPK	
1	1.5	11	25	25	12	820	230	40000	1600	8.0
2	1.2	3.5	11	3.5	61	540	130	27000	>30000	51
3	1.0	3.5	24	76	0.94	0.46	5100	>30000	>30000	0.94
4	3.5	36	130	260	19	2100	200	40000	1800	5.4
5	0.76	2.1	7.7	3.3	48	40	n.d.	40000	1300	63
6	0.62	3.8	2.6	3.3	3.3	580	250	>30000	9800	5.3
	IC_{50}, kinase assay, [nM][b]									
	PI3Kα	PI3Kβ	PI3Kγ	PI3Kδ	mTOR	[c]α542K/545K/1047R	VPS34	DNAPK		
1	33	661	708	451	89	63 / 136 / 36	8486	8567	2.6	
4	45	607	778	110	94	111 / 216 / 87	2581	6917	13	

[a]Dissociation constants (K_d) were determined using ScanMax technology (DiscoveRx)[26] with 11 point 3-fold serial dilutions of the indicated compounds. K_d is the mean value from experiments performed in duplicate, and were calculated from standard dose response curves using the Hill equation depicted in Methods (n≥2). A TreeSpot representation of a full kinase panel and kinase residual binding values are shown in Supporting Information, Figure S1 and Table S2 for all above compounds except compound **2**. [b]Prokinase activity assays of the indicated enzymes and PI3Kα mutants. [c]Inhibition of PI3Kα E542K, E545K, and H2047R mutant activities are indicated. For these values, the wild type PI3Kα reference IC_{50}s were 122 nM for **1** and 142 nM for **4**.

Chemistry

To achieve a balanced PI3K and mTOR inhibition, and to adjust physicochemical properties, a library of 4,6-dimorpholino-1,3,5-triazines substituted with various C-2-aryl moieties was prepared from 4,4'-(6-chloro-1,3,5-triazine-2,4-diyl)dimorpholine (**7**, Scheme 1). The chlorine was displaced by aniline or heteroaryl moieties using Suzuki cross-coupling reactions with boronic acid pinacol esters. The desired products were obtained in moderate to good yield (11-86%) depending on the used boronic acid pinacol ester derivative. Moreover, compound **1** was transformed by acetylation, diazotization followed by bromination and Sandmeyer reaction in order to obtain derivatives bearing different substituents at the C-2 pyridine (**17**-**21**). All final compounds were analyzed for purity by analytical HPLC (> 95%).

We have recently reported an optimized synthetic route to compound **1**[11]. This strategy allowed for rapid access to large quantities of **1** starting from cyanuric chloride (81% yield) for pre- and clinical development.

Scheme 1. Synthesis of C-2-aryl-substituted 4,6-dimorpholino-1,3,5-triazine analogs[a]

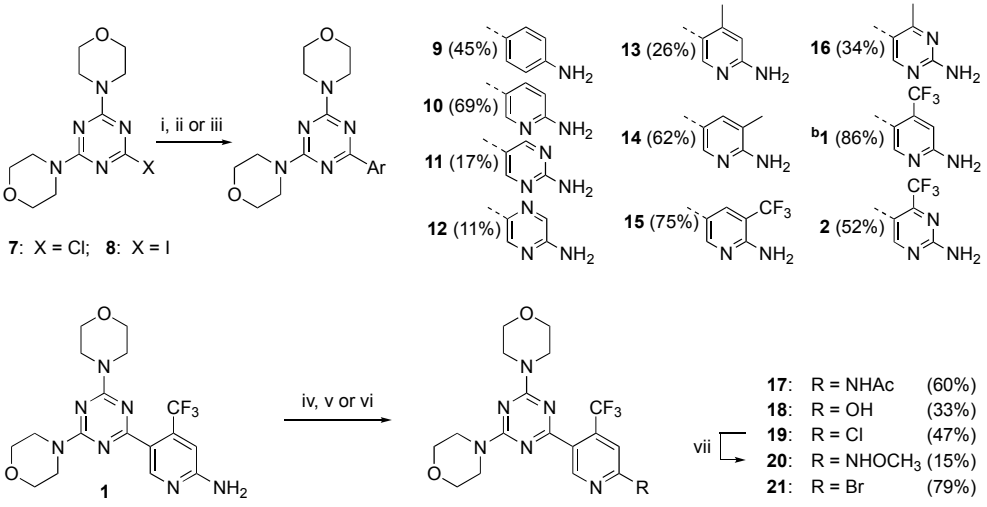

[a]Reagents and conditions: (i) ArBpin, XPhosPdG2 (cat.), K_3PO_4, dioxane / H_2O, 95 °C, 2-16 h, then HCl (aq.), 60 °C, 2-8 h; (ii) ArBpin, $Pd(dppf)Cl_2$ (cat.), Na_2CO_3, 1,2-dimethoxyethane / H_2O, 90 °C, 16 h; (iii) ArBpin, XPhosPdG2 (cat.), K_3PO_4, dioxane / H_2O, 95 °C, 2 h; (iv) AcCl, K_2CO_3, CH_2Cl_2, 0 °C → rt, 3.5 h; (v) HCl (conc.), $NaNO_2$, 0 °C → rt, 1 h, then CuCl, rt, 1 h; (vi) isopentyl nitrite, CH_2Br_2, rt, 5 min then $(CH_3)_3SiBr$, rt, 1 h; (vii) $CH_3ONH_2 \cdot HCl$, $NaHCO_3$, DMSO, 100 °C, 6 h. [b]Compound **1** was prepared according to the procedure recently reported[11]. ArBpin: boronic acid pinacol ester (the amino group was protected in certain cases).

Determination of cellular potency and PI3K vs. mTOR kinase activities

In the following studies, the role of the aryl moiety was investigated systematically for enzymatic activity and selectivity for class IA PI3K versus mTOR (Table 2). A first series of compounds including variations of nitrogen atoms number and position was prepared to study the effect of the polarity of the aryl group (**9**-**12**). Interestingly, **10** and **11** substituted with 2-aminopyridine and 2-aminopyrimidine, respectively, were both found to be active in cellular and enzymatic assays. The calculated PSA (polar surface area)-value for the pyridine-substituted **10** (PSA=103) was slightly lower as compared to pyrimidine **11** (PSA=115), predicting a better brain penetration for **10**. Therefore, pyridines were substituted with lipophilic substituents such as methyl and trifluoromethyl at pyridine C3-and C4-positions to generate compounds (**13**-**15**). Introduction of a C4-trifluoromethyl group significantly increased cellular potency and enzymatic targeting: compared with **13**, **1** showed excellent cellular activities, good potency *in vitro* (K_i for PI3Kα of 17 nM), targeted mutated forms of the catalytic PI3Kα subunit, and displayed the desired selectivity profile targeting PI3Kα>mTOR (K_i ratio of mTOR/p110α ~ 3.6 [~ 8.0 from KINOMEscan™, see Table 1]). On the contrary, introduction of a lipophilic substituent at the C3-position (methyl in **14** and trifluoromethyl in **15**) diminished binding to PI3Kα as well as to mTOR.

While compound **11**, bearing an unsubstituted 2-aminopyrimidine, turned out to be a balanced inhibitor for PI3Kα and for mTOR *in vitro*, (K_i mTOR/K_i PI3Kα ~2.3), a substitution at the pyrimidine C4-position with methyl (**16**) or trifluoromethyl (**2**) enhanced cellular and in vitro activity towards PI3Kα, and diminished affinity for mTOR, rising the mTOR/PI3Kα K_i ratio to ~16 to 25. Modifications at the C2-pyridine position of the most potent compound **1** were also investigated (**17**-**21**). These changes alter both the steric and the electronic properties of the amine group, and are likely to affect hydrogen bond interactions with the aspartate carboxy-groups in the affinity binding pocket (Asp841 and Asp836 in PI3Kγ). Hydroxylamine and amide moieties replacing primary amine functionality in **1** impaired binding to mTOR (K_i > 1 μM), and replacing the primary amine moiety by a hydroxylamine, amide, hydroxy or halide decreased cellular potency considerably. Compound **17** retained its affinity for PI3Kα in spite of an amide extension, likely due to a hydrogen bond of the amide carbonyl with Lys802 (Lys833 in PI3Kγ; in analogy to compound **26** in Ref. 27 [see also PDB ID 3IBE]).

Table 2. Direction of PI3K/mTOR selectivity with aromatic substituents for dimorpholino-triazine

Cmpd	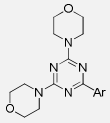	Cellular IC_{50} [nM][a,b]				*in vitro* K_i [nM][c]				
		pPKB/Akt	pS6	Growth A2058	Growth SKOV3	PI3Kα	mTOR	mTOR/PI3Kα	clogP[d]	PSA[d]
9	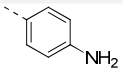	1744	1282	12630	8504	1513	396	0.26	2.45	89.6
10	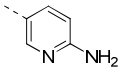	367	415	3819	742	123	110	0.89	2.23	103
11	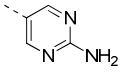	330	415	2161	270	46	106	2.34	1.39	115
12	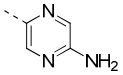	1283	817	9083	4428	911	185	0.20	1.31	115
13	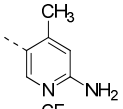	401	939	9113	1504	61	609	10.00	2.69	102
1	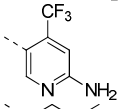	139	205	2333	237	17	62	3.60	3.11	102
14	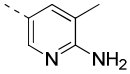	1620	1105	14210	6221	1205	241	0.20	2.69	102
15	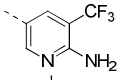	2370	1638	>20000	9213	4.3e6	284	6.5e-5	3.11	102
16	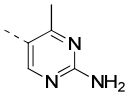	169	831	2934	342	13	224	17.60	1.56	115
2	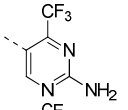	85	312	1636	73	8.1	203	25.10	2.67	115
20	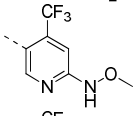	3303	5588	19200	4545	689	2539	3.70	3.09	97.8
17	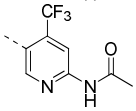	208	729	14480	11500	9.7	1213	125.00	3.22	105
18	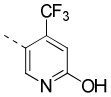	1.3e5	1.7e7	>20000	>20000	2299	n.d.	–	3.61	96.7
19	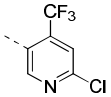	51971	1.1e6	4347	14050	32833	1.1e5	3.22	4.08	76.5
21	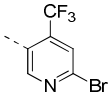	1.5e5	n.d.	3033	3654	n.d.	6.6e5	–	4.38	76.5

[a]Cellular phosphorylation of PKB/Akt on Ser473 and ribosomal S6 on Ser235/236 were analyzed in inhibitor treated A2058 melanoma cells using in-cell western detection. Each experiment performed in triplicate or as a multiple of n = 3. [b]IC_{50}s of A2058 or SKOV3 cell proliferation were determined from 10-point 2-fold serial dilutions (n=3). [c]Compounds were tested in a time-resolved FRET (TR)-assay (LanthaScreen), and inhibitor K_is were calculated for PI3Kα and mTOR as described in

methods. The mTOR/PI3Kα column depicts the ratio of compound-specific mTOR K_i over the K_i for PI3Kα. Each experiment performed at least twice or as a multiple of n = 2. [d]Marvin/JChem 16.10.17 was used for calculation of logP (partition coefficient) and PSA (polar surface area) values.

The SAR-study depicted above led to the identification of two potent compounds **1** and **2**, both substituted with a trifluoromethyl group on their aryl moiety**.** Both of them showed excellent potency for PI3Kα, cellular activity profiles, and a calculated logP-values of ~3. Compound **1** was investigated in more detail, as it displayed a mTOR/PI3Kα K_i selectivity ratio in the range of 3-8, while **2** had reduced impact on mTOR (Tables 1,2). An additional point in favor of compound **1** was a lower calculated PSA value of 102 as compared to 115 for **2**, predicting a better brain penetration for **1**.

Binding mode of compound 1 to PI3K and mTOR kinase

Binding of compound **1** to the PI3Kγ catalytic subunit p110γ ATP-binding site was confirmed by a 2.7 Å complex crystal structure, and identified key interactions of **1** with residues of p110γ. As reported for other morpholino-substituted PI3K inhibitors including compound **4**[11,19], one morpholine of **1** forms a hydrogen bridge with the backbone amide of Val882, a well-known and crucial interaction[28]. The compound **1**/PI3Kγ complex crystal structure (PDB ID code: 5OQ4; Table S1) also showed that the amino group of the 2-amino-4-(trifluoromethyl)pyridine moiety forms H-bonds with Asp836, Asp841 and Asp964 (Figure 2A). Given the high homology of class I PI3K catalytic pockets, and the nanomolar in vitro dissociation constants of **1** for all class I PI3Ks (Table 1), an identical binding mode for all PI3K isoforms can be assumed. Besides the high affinity for class I PI3K isoforms (highest affinity for PI3Kα), compound **1**'s affinity for mTOR kinase is comparable to PI3Kβ, PI3Kγ and PI3Kδ (Table 1).

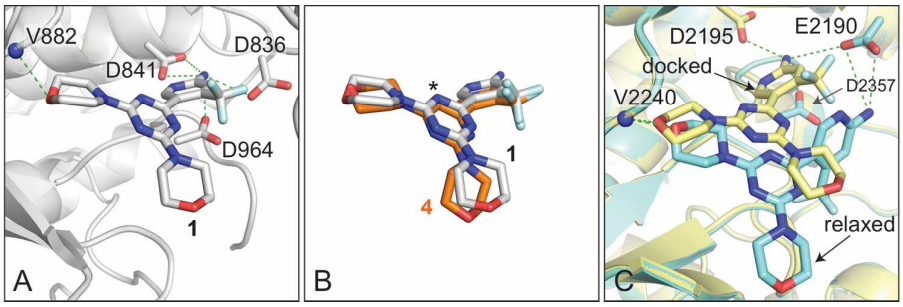

Figure 2. Interactions of **1** with the ATP-binding site of PI3Kγ catalytic subunit p110γ and mTOR kinase. **A)** Crystal structure of **1** in PI3Kγ with a resolution of 2.7Å (PDB ID code: 5OQ4; Table S1). Compound **1** interacts with the hinge

valine V882 in PI3Kγ, and its heteroaryl amine function forms hydrogen bonds with the carboxyl groups of aspartates D836, D841, and D964. **B)** Overlay of the compound **1**/PI3Kγ complex coordinates with the compound **4**/PI3Kγ data from PDB accession code 3SD5.[19] The pyrimidine core nitrogen atom positions are corrected for the orientation as proposed in Ref. 11 (* denotes the position of C-H in compound **4**); the two molecules are oriented exactly as in **A). C)** The coordinates of a mTOR kinase/PI103 complex resolved to 3.6 Å (PDB code: 4JT6; docked, yellow) and mTOR at a resolution of 3.2 Å (PDB code: 4JSN; relaxed, turquoise) were used to dock **1** into the ATP-binding site of mTOR kinase. The yellow structure represents the results of a manual pre-docking process (docked) where PI103 was replaced by **1** with subsequent energy minimization; the turquoise structure represents the best fit of dynamic docking procedures to 4JSN (relaxed starting conditions). Dotted lines indicate proposed H-bond interactions.

The current compound **1**/PI3Kγ X-ray crystal structure combined with our previous structural studies on **4** and an asymmetrically substituted triazine (PIKiN3, PDB ID 5JHB),[11] underlines the importance of Asp836, Asp841 and Asp964, and associated structured water molecules, for the binding of this compound class. Changes in the basicity of the amino-heteroaryl (2-amino-4-(trifluoromethyl)pyridine in **1** are therefore expected to affect the affinity for PI3K, as it was the case for 2-amino-pyrimidine **2**. The situation in the mTOR catalytic pocket is less well defined: i) modelling compound **1**/mTOR interactions starting with a pre-docked inhibitor generate an interaction pattern similar to PI3K, where carboxyl groups of Asp2357, Glu2190, and Asp2195 are at a distance of 3.5 to 4 Å from the hetero-aryl amino group and could execute hydrogen bonding; ii) starting with less constraints, the inhibitor is slightly displaced by docking procedures, and the sole residue in hydrogen bonding distance remains Glu2190. Although less conventional, the latter structure offers some explanation for the differential effects of hetero-aryl modifications for PI3K and mTOR affinity shown in Table 2.

On and off target activities

In line with its activities against PI3K and mTOR, compound **1** induced a G1 cell cycle arrest in A2058 melanoma cells (mutated B-Raf, loss of PTEN) and SKOV3 cells (PI3Kα mutated at H1047R), which have both constitutively activated PI3K/mTOR signaling pathways. In contrast, compound **4** triggered a mitotic arrest and cells accumulated in G2/M or subG1 (Figure 2), which is in agreement with the reported binding of **4** to the colchicine-binding site of tubulin.[11] In spite of compound **4**'s off-target effect, the compound attenuated PI3K and mTOR signaling as determined by protein kinase B (PKB/Akt) phosphorylation on Ser473 and Thr308, and S6 kinase (S6K, Thr389) and S6 phosphorylation on Ser235 and Ser236. Here, **4** closely matched the action of **1**,

5, **6**, **3** and **2**, while rapamycin by its specific action on TORC1 triggered an upregulation of PI3K activity, which is in agreement with earlier observations.[29]

To validate the specificity of **1**, the compound was tested in a KINOMEScan™ panel for interactions with a wide range of protein (>400) and lipid kinases in parallel with **4**, **5**, **6** and **3**. At 10 μM concentration **1**, **4**, **5** and **3** did show negligible interference with protein kinase activities (Figure S1, Table S2), while the dual PI3K/mTOR kinase inhibitor **6** displayed multiple hits. Compound **1** reached excellent selectivity scores of S(35) =0.025, S(10)= 0.018, as calculated according to Ref. 30.

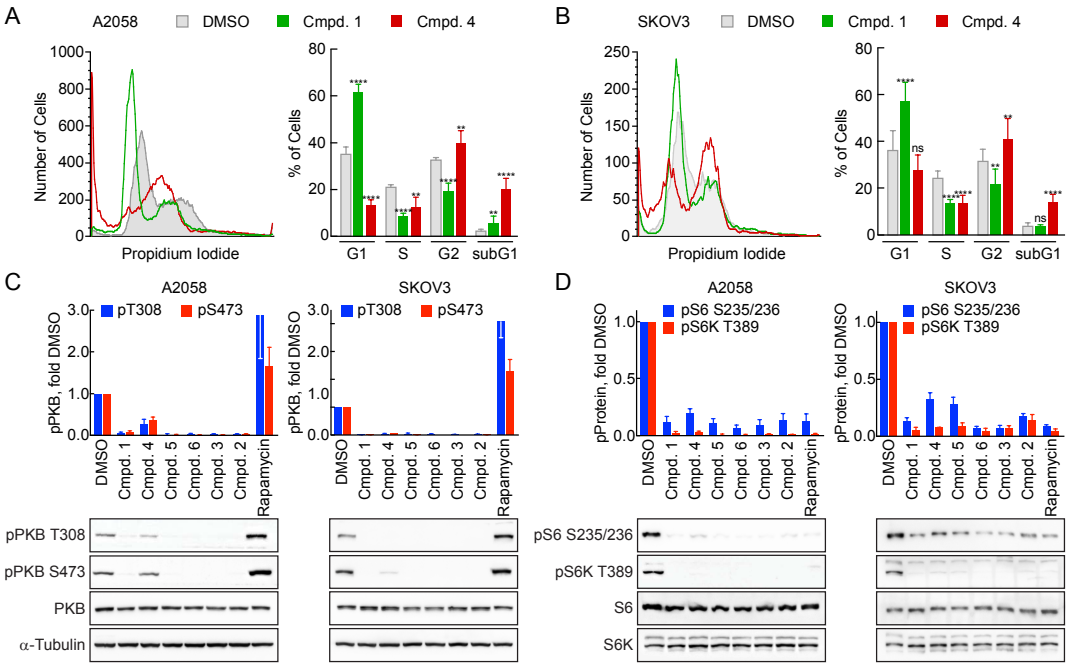

Figure 3. Action of indicated compounds on cell cycle and PI3K and mTOR signaling. Cell cycle distribution of A2058 **(A)** and SKOV3 (**B**) cells after 24 h exposure to 5 μM (**A**) or 2 μM (**B**) of indicated drugs (**1**, green; **4**, red) or DMSO. After drug exposure cells were collected, fixed, permeabilized and the DNA stained using propidium iodide. Cell cycle profiles were acquired by fluorescence activated cell sorting. *Left panels:* Examples of cell cycle histograms. *Right panels*: Quantification of cells in cell cycle phases G1, S, G2/M and sub G1 (as % of total, n=9, mean ± SD, one way ANOVA test with Dunnett's multiple comparison test for each cell cycle phase related to DMSO; ns: not significant, ** p>0.0021, **** p> 0.0001). **C**, **D**) A2058 or SKOV3 cells were exposed to 1 μM drug (Rapamycin 100 nM) for 1h, subsequently lysed and the denatured lysates subjected to SDS-PAGE, Western blotting and immune-detection. **C**) Detection of total and phosphorylated (pT308 and pS473) PKB/Akt, and α-tubulin (*left*: A2058, *right*: SKOV3). *Top:* Quantification of phospho-PKB/Akt levels related to DMSO control (blue: pT308, red: pS473, n=3, mean ± SEM). **D**) Detection of total and phosphorylated (pS235/236) ribosomal protein S6, and of total and phosphorylated (S6K T389) S6 Kinase (*left*: A2058, *right*: SKOV3). *Top:*

Quantification of phospho-protein levels, related to DMSO control (blue: phospho S6, red: phospho S6K, n=3, mean ± SEM).

The impact of compound **1** on cell proliferation was analyzed in four independent human tumor cell line collections of different tissue origin (NCI60;[31] NTRC, Netherlands; Horizon Discoveries, UK; Clovis, UK; 135 different cell lines in total). Combined across the four cell panels the mean half-maximal growth inhibition (GI_{50}) was reached at ca. 0.7 µM (median: ca. 0.5 µM) of **1** as depicted in Figure 4.

We have previously compared IC_{50}-independent parameters such as Hill slopes of proliferation inhibition curves and dose-dependent induction of nuclear condensation and histone H3 phosphorylation in a 44 cell line panel treated with either **1**, **4**, **5**, or **6**, which showed a co-clustering of the PI3K inhibitors **1**, **5**, and **6**, and grouped **4** with inhibitors of mitosis such as colchicine, nocodazole and MTD147 – a microtubule-binder derived from **4**,[11] corroborating that **1** is free of the microtubule-binding off-target action of **4**.

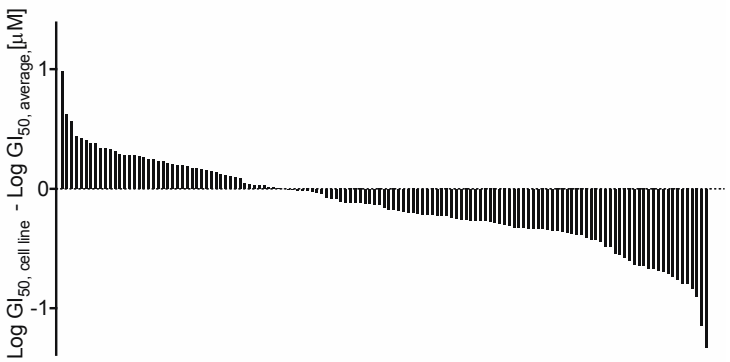

Figure 4. Cell proliferation in response to **1** represented as a waterfall blot. Concentrations of half-maximal growth inhibition (GI_{50}) for **1** were obtained from dose-response growth curves derived from 4 different tumor cell line panels (a total of 135 cell lines; if a cell line was contained in several panels its GI_{50} was averaged). Individual GI_{50} of a cell line was related to the mean GI_{50} of all cells lines, and cell lines were sorted by lowest to highest sensitivity for **1** from left to right. Individual cell lines and values for the four cell panels are given in Table S3.

To evaluate other off-target effects, compound **1** was tested at 10 µM in a CEREP BioPrint panel, where no or only very weak competition with radio ligands for cell surface and nuclear receptors, membrane channels, transporters (Table S4) and enzyme activities of kinases, proteases and phosphodiesterases (Table S5) were detected. Altogether, **1** qualifies as a specific pan-class I PI3K inhibitor without predicted off-target effects.

Pharmacological parameters of compound 1

Before translation of the in vitro and cellular activities to in vivo tumor models, pharmacological properties and metabolic stability of **1** were assessed. Compound **1** showed little clearance when exposed to rat, dog and human liver microsomes, with a quicker turnover of **1** in mouse liver microsomes, where 40% of the compound was eliminated within 30 min (Table 3A). Stability in microsome assays were matched with clearance and half-live measurements in human, cynomolgus monkey, rat, dog and mouse hepatocyte cultures, where **1** showed a low clearance in all species except for mouse. In the presence of human hepatocytes, the half-life of compound **1** was 9.4 h, and ca. 45 min in mouse hepatocytes (Table 3B).

Table 3A: Stability in liver microsomes of compound 1

	% remaining in liver microsomes[a]			
Cmpd \ species	**Human**	**Rat**	**Dog**	**Mouse**
1	84.6 ± 2.2	99.9 ± 0.5	92.4 ± 1.6	60.7 ± 4.6
7-EC[b]	7.45 ± 0.8	28.5 ± 3.1	1.8 ± 1.0	1.5 ± 0.03
Propranolol[b]	54.8 ± 6.7	2.9 ± 0.1	30.1 ± 2.6	6.8 ± 0.9

[a]percentage of compound remaining after 30 min (mean ± SD, n=2); [b]Assay reference compounds: 7-EC, 7-Ethoxycoumarin.

Table 3B: Stability of compound 1 in hepatocyte cultures

Cmpd \ species		**Human**	**Monkey**	**Rat**	**Dog**	**Mouse**
1	[a]CL_{int}	2.5 ± 0.4	3.5 ± 0.1	1.9 ± 0.1	2.4 ± 0.1	30.3 ± 0.1
	$t_{1/2}$ **[min]**	562.6 ± 95.5	396.4 ± 16.0	731.7 ± 54.5	577.6 ± 0.1	45.7 ± 0.2
7-EC[b]	CL_{int}	37.8 ± 0.8	61.1 ± 3.5	16.0 ± 0.8	151.4 ± 2.8	180.3 ± 0.1
	$t_{1/2}$ **[min]**	36.7 ± 0.8	22.7 ± 1.3	86.8 ± 4.6	9.2 ± 0.2	7.7 ± 0.1
7-HC[b]	CL_{int}	98.2 ± 5.1	92.5 ± 3.5	192.8 ± 14.4	178.3 ± 0.7	188.1 ± 8.6
	$t_{1/2}$ **[min]**	14.1 ± 0.7	15.0 ± 0.6	7.2 ± 0.5	7.8 ± 0.1	7.4 ± 0.3

[a]CL_{int} [µl/min/10^6 cells]; $t_{1/2}$, [min]; [b]Assay reference compounds: 7-EC, 7-Ethoxycoumarin; 7-HC, 7-Hydroxycoumarin; Results are expressed as Mean ± SD, n=2.

Subsequently, in vivo pharmacological parameters were determined in female CD-1 mice, female Sprague-Dawley rats and male Beagle dogs to assess optimal dosing schedules for efficacy studies. Compound **1** was delivered either by a single intravenous (5 mg/kg) bolus or a single oral application (10 mg/kg). Drug levels in extracts of plasma, brain and liver were determined by LC-MS/MS (Figure 5; PK parameters are summarized

in Table 4). In female mice, plasma concentrations of **1** depended on the drug administration route, resulting in half-lives of ca. 13-36 min for p.o. administration vs. 9-10 min for i.v. administration. The fact that oral administration yielded similar concentrations of **1** in brain and plasma samples, illustrates that compound **1** readily passes the blood brain barrier. In mice, both p.o. and i.v. application routes showed a rapid drop below 200 ng/ml (ca. 0.5 µM, Figure 5A) of **1** within <1 h (i.v.) to <2 h (p.o.) post administration, which reflects the time point when the drug reaches the median GI_{50} determined in tumor cell lines.

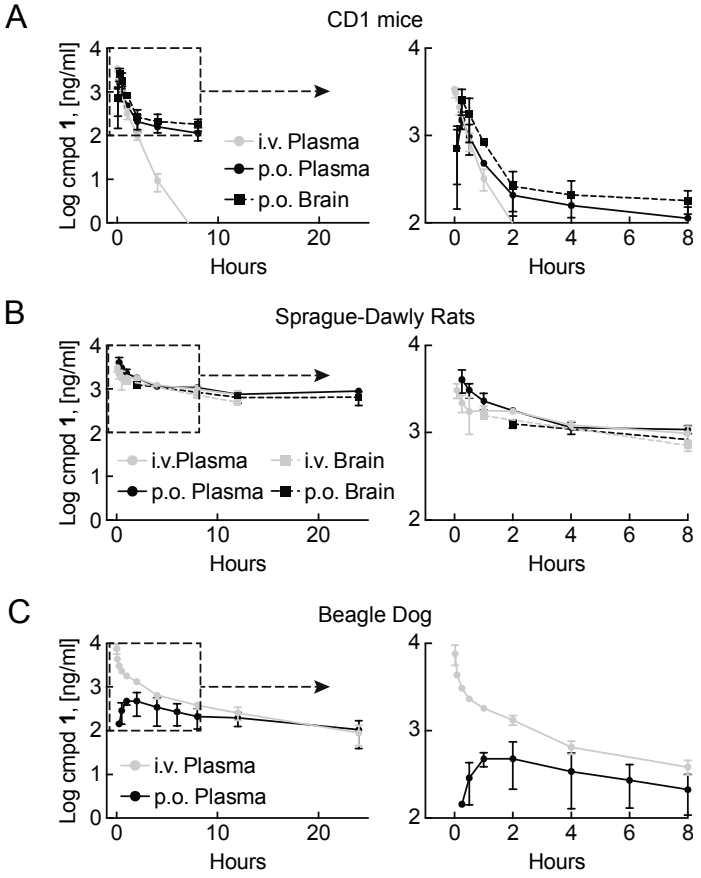

Figure 5. PK/PD assessment of **1** in mice, rats and dogs: time course of **1** abundance in vivo. Compound **1** was administered in all species as single dose either per os (p.o., 10 mg/kg) or via intravenous injection (i.v., 5 mg/kg). At indicated time-points **1** was extracted from tissue and its abundance determined using HPLC/MS-MS. **A)** Levels of **1** in CD1-mice tissue. Right graph: Zoomed view on early time-points, indicated in left graph by dashed square (n=3, mean± SD). **B)** Concentrations of **1** in tissues from Sprague-Dawly rats. Right graph: Zoomed view on early time-points, indicated in left graph by dashed square (n=3, mean± SD). **C)** Plasma levels of **1** in male Beagle dogs. Panels on the right: zoomed in to dotted line boxes to visualize early time-points (n=3, mean± SD).

In female rats a single oral dose (10 mg/kg) achieved similar drug levels as a single intravenous injection (5 mg/kg) with regard to C_{max} (see Table 4). The half-life of 5 to 8 h, and an $AUC_{0.25\text{-}12}$ of around 14'000 hr.ng/ml contributed to an excellent oral bioavailability of **1** (>50%). Twenty-four hours post p.o. administration, plasma levels of **1** were still > 2 µM (800-1000 ng/ml). Moreover, after 1 to 2 h exposure to **1**,

drug levels in rat brain samples were comparable to plasma levels (Fig. 5B), confirming rapid access of **1** to the brain.

Male Beagle dogs, exposed to **1** at 10 mg/kg p.o., showed maximal drug plasma concentrations C_{max} of 583 ng/ml (approx. 1.5 μM) after 60 to 90 min and a half-life of >7 h, which results in drug levels of approximately 0.38 μM (150 ng/ml) after 24 h. Intravenous delivery of 5 mg/kg of **1** resulted in high immediate concentrations (>7000 ng/ml after 1 min.), and plasma levels decreased within 8 hours to similar concentrations as observed for oral dosing (Fig. 4C). The oral bioavailability in male Beagle dogs was estimated to be 23%.

In vitro and in vivo toxicokinetic parameters were assessed and are summarized in Table S6. In rodents and beagle dogs, compound **1** showed moderate but reversible target organ toxicity, which is expected for this drug class and mechanism of action. Altogether the PK studies in the three models show rapid absorption of **1** and good oral bioavailability. Except for mice with a rapid clearance of **1**, the late phase concentrations of **1** in rats and dogs are in the expected range of predicted efficacy, independent of the administration route, and are already reached after a single dose. The collected parameters are compatible with oral dosing in humans once daily (QD).

Altogether, compound **1** displays a superior solubility (Table S7) as compared with compound **2**, is orally bioavailable and brain penetrable, and does not display a microtubule-binding off-target effect like compound **4**.[11]

Table 4: PK analysis of 1 in plasma of mice, rats and dogs

	Female CD-1 Mouse		**Female Sprague-Dawley Rats**		**Male Beagle Dog**	
Route	i.v.	p.o.	i.v.	p.o.	i.v.	p.o.
Dose [mg/kg]	5	10	5	10	5	10
C_{max} [ng/ml]	3084 ± 379	1514 ± 334	3047 ± 557	4028 ± 1179	8760	583
T_{max} [min]	5	15	5	15	5	120-240
$t_{1/2}$ [h]	0.15-0.33	0.22-0.60	5.6-8.2	5.6	7.6	8.6
AUC [h*ng/ml]	1583	2151	13974	15313	12500	6395
	AUC_{0-8h}	AUC_{0-8h}	$AUC_{0.25-12h}$	$AUC_{0.25-12h}$	$AUC_{0.25-24h}$	$AUC_{0.017-24h}$
Cl [ml/h/kg]	3180		266		411	
BA [%]		68		55		23

i.v. intravenous (5 mg/kg); p.o.: per os (10 mg/kg); C_{max}: maximal concentration, T_{max}: time of maximal concentration in hours; $t_{1/2}$: half-life elimination in hours; AUC: Area under curve, Cl: clearance; BA: bioavailability; (n=3, mean ± SD for each time-point, species and route)

Efficacy models

Due to the short half-live of compound **1** in mice, a PC3 xenograft model in nude rats was used to assess the anti-proliferative effects of **1** in vivo. Rats were injected with 2 x 10^7 human PC3 prostate cancer cells into one flank and randomized after 16 days. From day 17 the control group received vehicle once daily. Compound **1** was orally administered at 5 mg/kg, 10 mg/kg (both daily, QD1) or 15 mg/kg [5 consecutive days, 2 days off drug (QDx5, 2 days off)] for 28 days to match the timelines of regulatory toxicology studies. A vinorelbine-treated group (2.5 mg/kg i.v. weekly) was included as a "standard of care" control, with best treated–to-control ratios (T/C) of 17%.

Treatment with **1** led to significant tumor size reductions: tumor growth was inhibited dose-dependently (best T/C of 31- 12%, Fig. 6A). Compound **1** was best tolerated at 5 mg/kg without significant body weight changes (Fig. 6B). At 10 mg/kg **1** caused a reduction of body weight, which accumulated to a reduction of 15% after 28 days of treatment. Similarly, 15 mg/kg of **1** led to body weight loss after 5 days of treatment, which was reversible during the recovery period. After 28 days of drug exposure (day 44 of the experiment), animals with body weight loss fully recovered within a treatment-free period (day 45- 50) without overt signs of tumor cell proliferation. In a subsequent treatment period tumor growth remained inhibited and body weight loss was only observed in the 15 mg/kg group.

As shown in Figure 6C, C_{max} of compound **1** is reached 15 min after a p.o. single dose in PC3-tumor bearing nude rats, and triggered a rapid and dose-dependent rise in plasma insulin and glucose levels (Figure 6D-F), which are reliable markers for the drugs on-target action, as reported for other PI3K inhibitors targeting the PI3Kα isoform.[32]

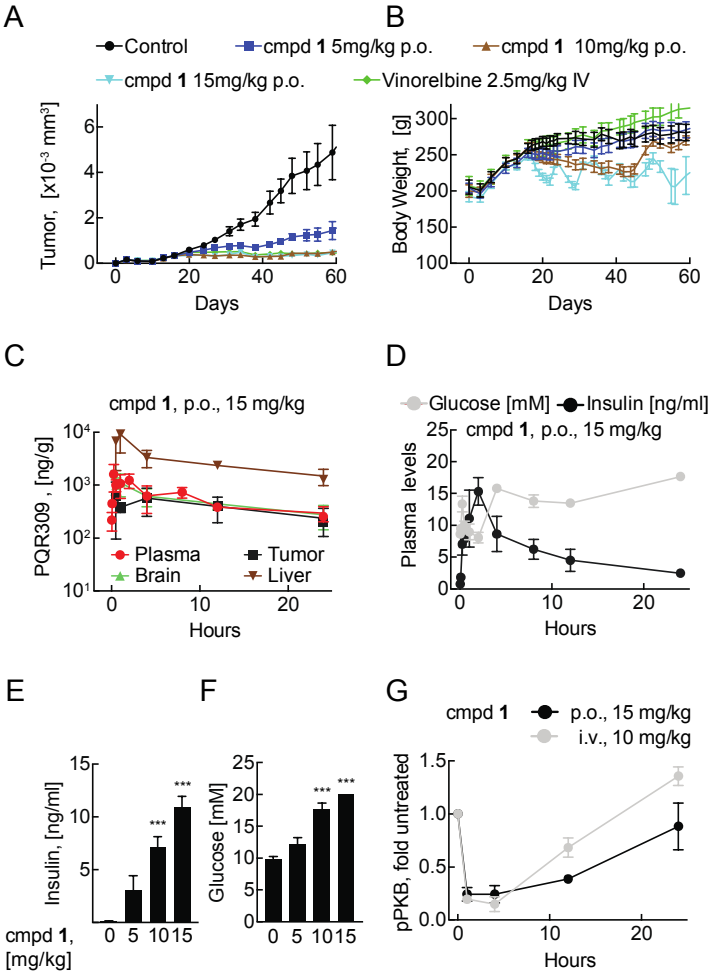

Figure 6. Efficacy model for anti-tumor activity of **1** in PC3 xenografts in nude rats. **A)** Tumor volume: indicated amounts of **1** (p.o., daily) or Vinorelbine (i.v., weekly) were given from day 17-44 and from day 51-58 after tumor inoculation (see materials and methods; n = 4-8, mean± SEM). **B)** Body weight changes in nude rats (treated as in (A), n = 4-8, mean ± SEM). **C)** Time course of **1** abundance in nude rats. Compound **1** was administered as single dose per os (p.o., 15 mg/kg). At indicated time-points **1** was extracted from tissue and its abundance determined using HPLC/MS-MS (n=3, mean± SD). **D)** Time course of blood glucose and insulin levels tumor bearing rats after a single dose of **1** (15 mg/kg p.o.; n=3, mean ± SEM; except for time-points with values above detection limit). **E)** Plasma insulin and **F)** Plasma glucose concentrations on day 57 of the efficacy model, 4 h after the last administration of **1** at indicated doses (n = 6-7, mean ± SEM, for insulin levels below detection level – values were set constant to 0.04 [lowest measured value], for glucose levels above quantification limit, levels were set 20 [upper quantification limit of kit]). **G)** Time course of phosphorylation of Ser473 in PKB/Akt in PC3 tumor xenograft lysates after a single dose of **1** (15 mg/kg p.o. or 10 mg/kg i.v.). Lysate were subjected to SDS-PAGE and western blotting. Phosphorylated Ser473 levels were corrected for total PKB/Akt levels and compared to vehicle-treated xenografts (n=3, mean± SEM).

To further corroborate on-target activity of compound **1** in vivo, phosphorylation of pPKB/AKT was measured in tumor-derived cell lysates. A single dose of **1** (15 mg/kg p.o. or 10 mg/kg i.v.) rapidly reduced pPKB/AKT levels as compared to untreated control mice up to 12 h (Figure 6G), which matches high levels of **1** in the xenograft tumors at early time points (Figure 6C). After 24 h, PI3K signaling fully recovered, correlating with a decrease of compound **1**'s concentration in tissue and tumors. Pharmacokinetics in plasma, brain and tumor samples were very similar, suggesting that **1** distributes rapidly, and targets PI3K and mTOR in tumor and

tissues. Proportionally elevated levels of **1** were detected in the liver, without signs of liver toxicity. The fast reversibility of PI3K inhibition might be of advantage in patients, where mechanism-based adverse effects are expected to resolve with falling drug levels. Moreover, it has been observed that tumor cells reduce cell size in response to PI3K inhibitors, while normal hepatocytes do not show mass reduction.[17] This, and the observation that interruption of drug administration (see 15 mg/kg schedule above) leads to body weight recovery but not tumor regrowth, suggests that PI3K inhibition triggers latency in tumor growth that allows for the development of intermittent scheduling protocols. To validate this treatment scheme, PC3 tumor-bearing nude rats were treated every second, third and fourth day with 15 mg/kg p.o., which yielded a comparable efficacy, but substantially alleviated the loss of body weight (Figure S2).

CONCLUSION

The preclinical results presented here document that compound **1** is a highly selective pan-PI3K inhibitor with a balanced targeting of mTOR kinase. Compound **1**'s potent anti-proliferative action in vitro and anti-tumor activity in vivo, paired with mild and reversible, mostly mechanism-based toxicities have validated the molecule as a clinical candidate. Compound **1** passed phase I studies and is now in phase II studies in relapsed and refractory lymphoma and advanced solid tumors (clinicaltrials.gov).

Experimental Section

General Information.

Reagents were purchased at the highest commercial quality from Acros, Sigma-Aldrich or Fluorochem and used without further purification. Solvents were purchased from Acros Organics in AcroSeal® bottles over molecular sieves. Column chromatographic purifications were performed on Merck KGaA silica gel (pore size 60 Å, 230-400 mesh particle size). Cross coupling reactions were carried out under nitrogen atmosphere in anhydrous solvents and glassware was oven dried prior to use. TLC plates were obtained from Merck KGaA (Polygram SIL / UV254, 0.2 mm silica with fluorescence indicator) and UV light (254 nm) was used to visualize the respective compounds. ^{1}H, ^{19}F and ^{13}C NMR spectra were recorded on a Bruker Avance 400 spectrometer. NMR spectra were obtained in deuterated solvents such as $CDCl_3$ or $(CD_3)_2SO$. The chemical shift (δ values) are reported in ppm and corrected to the signal of the deuterated solvents (7.26 ppm (^{1}H NMR) and 77.16 ppm (^{13}C NMR) for $CDCl_3$; and 2.50 ppm (^{1}H NMR) and 39.52 ppm (^{13}C NMR) for $(CD_3)_2SO$). ^{19}F NMR spectra were calibrated relative to $CFCl_3$ ($\delta = 0$ ppm) as external standard. When peak multiplicities are reported, the following abbreviations are used: s (singlet), d (doublet), dd (doublet of doublets), m (multiplet), br (broadened). Coupling constants, when given, are reported in Hertz (Hz). High resolution mass spectra (HRMS) were recorded on a Thermo Fisher Scientific LTQ Orbitrap XL (ESI-MS) spectrometer. MALDI-ToF mass spectra were obtained on a Voyager-De™ Pro measured in *m/z*. The chromatographic purities of the final compounds were determined by high performance liquid chromatography (HPLC) analyses on an Ultimate 3000SD System from ThermoFisher with LPG-3400SD pump system, ACC-3000 autosampler and column oven, and DAD-3000 diode array detector. An Acclaim-120 C18 reversed-phase column from ThermoFisher was used as stationary. Gradient elution (5:95 for 0.2 min, 5:95 → 100:0 over 10 min, 100:0 for 3 min) of the mobile phase consisting of CH_3CN / MeOH:$H_2O_{(10:90)}$ was used at a flow rate of 0.5 ml / min at 40 °C. The purity of all final compounds was > 95% pure.

General procedure 1.

4,4'-(6-Chloro-1,3,5-triazine-2,4-diyl)dimorpholine (**7**, 1.0 eq.), the respective boronic acid pinacol ester (1.0-1.5 eq.), potassium phosphate tribasic (3.0 eq.) and chloro(2-dicyclohexylphosphino-2',4',6'-triisopropyl-1,1'-biphenyl)[2-(2'-amino-1,1'-biphenyl)]palladium(II) (XPhos Pd G2, 0.05-0.10 eq.) were charged in a flask. Under nitrogen atmosphere, 1,4-dioxane (approx. 1 ml / 0.2 mmol) and deionized H_2O (approx.

1 ml / 0.4 mmol) were added and the resulting mixture was placed into an oil bath pre-heated to 95 °C and stirred at this temperature for 2-16 hours. After completion of the reaction, the mixture was allowed to cool to room temperature, before addition of a 3 M aqueous HCl-solution and then heated at 60 °C for 2-8 hours. Then the mixture was allowed to cool to room temperature, the pH was adjusted to 8-9 by addition of a 2 M aqueous NaOH-solution and the aqueous layer was extracted with ethyl acetate (3 x). The combined organic layers were dried over anhydrous Na_2SO_4, filtered and the solvent was evaporated under reduced pressure. The crude product was purified by column chromatography on silica gel.

General procedure 2.

To a solution of the respective boronic acid pinacol ester (4.0 eq.), [1,1'-bis(diphenylphosphino)ferrocene]dichloropalladium(II) (0.05 eq.) and 4,4'-(6-chloro-1,3,5-triazine-2,4-diyl)dimorpholine (**7**, 1.0 eq.) in 1,2-dimethoxyethane (approx. 1 ml / 0.2 mmol) under nitrogen atmosphere, a 2 M aqueous Na_2CO_3-solution (3.0 eq.) was added. The resulting reaction mixture was heated at 90°C for 16 h. Then the mixture was allowed to cool to room temperature, poured onto an aqueous saturated NH_4Cl-solution and the aqueous layer was extracted with ethyl acetate (3x). The combined organic layers were washed with deionized H_2O, dried over anhydrous Na_2SO_4, filtered, and the solvent was evaporated to dryness under reduced pressure. The crude product was purified by column chromatography on silica gel.

General procedure 3.

N,N-Dimethylformamide dimethyl acetal (1.5 eq.) and the respective amine (1.0 eq.) were dissolved in tetrahydrofuran (approx. 1 ml / 0.3 mmol) and the resulting reaction mixture was stirred at 70 °C overnight. The solvent was evaporated under reduced pressure and the residue was triturated with acetonitrile (3x) before it was dried under *vacuum*.

5-(4,6-Dimorpholino-1,3,5-triazin-2-yl)-4-(trifluoromethyl)pyridin-2-amine (1) was prepared according to the reported procedure in Ref. 11.

5-(4,6-Dimorpholino-1,3,5-triazin-2-yl)-4-(trifluoromethyl)pyrimidin-2-amine (2) was prepared according to general procedure 1 from 4,4'-(6-chloro-1,3,5-triazine-2,4-diyl)dimorpholine (**7**, 300 mg, 1.05 mmol, 1.0 eq.) and 5-(4,4,5,5-tetramethyl-1,3,2-dioxaborolan-2-yl)-4-(trifluoromethyl)pyrimidin-2-amine (455 mg, 1.58 mmol,

1.5 eq.). Purification by column chromatography on silica gel (cyclohexane / ethyl acetate 2:3 → 3:2) gave product **2** as a colorless solid (225 mg, 546 µmol, 52%). **^{1}H NMR** (400 MHz, $CDCl_3$): δ 8.94 (s, 1 H), 5.65 (br s, 2 H), 3.39-3.78 (m, 8 H), 3.76-3.69 (m, 8 H); **^{19}F{^{1}H} NMR** (376 MHz, $(CD_3)_2SO$): δ − 63.8 (s, 3 F); **^{13}C{^{1}H} NMR** (101 MHz, $CDCl_3$): δ 168.5 (s, 1 C), 164.7 (s, 2 C), 163.1 (s, 1 C), 162.7 (s, 1 C), 154.6 (q, $^2J_{C,F}$ = 35 Hz, 1 C), 121.1 (s, 1 C), 120.8 (q, $^1J_{C,F}$ = 276 Hz, 1 C), 66.9 (s, 4 C), 43.7 (s, 4 C); **ESI-HRMS** (*m/z*): $[M + H]^+$ calc. for $C_{16}H_{20}F_3N_8O_2$, 413.1656; found: 413.1662; **HPLC**: t_R = 7.39 min (> 99.9% purity).

4,4'-(6-Chloro-1,3,5-triazine-2,4-diyl)dimorpholine (7) was prepared according to Ref. 11.

4,4'-(6-Iodo-1,3,5-triazine-2,4-diyl)dimorpholine (8). To an aqueous hydriodic acid solution (57 wt. %, 2.00 ml, 15.2 mmol, *excess*) diluted with deionized H_2O (2.00 ml), 4,4'-(6-chloro-1,3,5-triazine-2,4-diyl)dimorpholine (**7**, 500 mg, 1.75 mmol, 1.0 eq.) was added at 0 °C. The reaction mixture was allowed to warm to room temperature overnight and then poured onto a 1 M aqueous NaOH-solution. The product was extracted with ethyl acetate (3 x). The combined organic layers were dried over anhydrous Na_2SO_4, filtered and the solvent was evaporated under reduced pressure. The residue was purified by column chromatography on silica gel (cyclohexane / ethyl acetate 1:0 → 1:1) to afford product **8** as a colorless solid (409 mg, 1.08 mmol, 61%). **^{1}H NMR** (400 MHz, $CDCl_3$): δ 3.87-3.63 (m, 16 H); **^{13}C{^{1}H} NMR** (101 MHz, $CDCl_3$): δ 162.1 (s, 2 C), 140.6 (s, 1 C), 66.8 (s, 4 C), 44.0 (s, 4 C); **MALDI-MS**: *m/z* = 378.1 ($[M + H]^+$).

4-(4,6-Dimorpholino-1,3,5-triazin-2-yl)aniline (9) was prepared according to general procedure 1 from 4,4'-(6-chloro-1,3,5-triazine-2,4-diyl)dimorpholine (**7**, 150 mg, 525 µmol, 1.0 eq.) and *tert*-butyl (4-(4,4,5,5-tetramethyl-1,3,2-dioxaborolan-2-yl)phenyl)carbamate (**22**, 250 mg, 783 µmol, 1.5 eq.). Purification by column chromatography on silica gel (cyclohexane / ethyl acetate 1:0 → 3:2) gave product **9** as a colorless solid (80.9 mg, 236 µmol, 45%). **^{1}H NMR** (400 MHz, $CDCl_3$): δ 8.22 (d, $^3J_{H,H}$ = 8.7 Hz, 2 H), 6.69 (d, $^3J_{H,H}$ = 8.7 Hz, 2 H), 3.99-3.81 (m, 10 H), 3.79-3.72 (m, 8 H); **^{13}C{^{1}H} NMR** (101 MHz, $CDCl_3$): δ 170.3 (s, 1 C), 165.3 (s, 2 C), 149.7 (s, 1 C), 130.1 (s, 2 C), 127.5 (s, 1 C), 114.2 (s, 2 C), 67.0 (s, 4 C), 43.7 (br s, 4 C); **MALDI-MS**: *m/z* = 343.2 ($[M + H]^+$); **HPLC**: t_R = 7.27 min (> 99.9% purity). The spectroscopic data are consistent with previous literature reports.[34]

5-(4,6-Dimorpholino-1,3,5-triazin-2-yl)pyridin-2-amine (10) was prepared according to general procedure 2 from 4,4'-(6-chloro-1,3,5-triazine-2,4-diyl)dimorpholine (**7**, 200 mg, 702 µmol, 1.0 eq.) and 2-aminopyridine-5-boronic acid pinacol ester (616 mg, 2.80 mmol, 4.0 eq.). Purification by column chromatography on silica gel (dichloromethane / methanol 9:1) gave compound **10** as a colorless solid (166 mg, 483 µmol, 69%). **^{1}H NMR** (400 MHz, $CDCl_3$): δ 9.07 (d, $^4J_{H,H}$ = 2.3 Hz, 1 H), 8.37 (dd, $^3J_{H,H}$ = 8.7 Hz, $^4J_{H,H}$ = 2.3 Hz, 1 H), 6.50 (d, $^3J_{H,H}$ = 8.6 Hz, 1 H), 4.71 (br s, 2 H), 3.88 (br s, 8 H), 3.79-3.71 (m, 8 H); **^{13}C{^{1}H} NMR** (101 MHz, $CDCl_3$): δ 169.2 (s, 1 C), 165.1 (s, 2 C), 160.4 (s, 1 C), 150.0 (s, 1 C), 137.9 (s, 1 C), 123.6 (s, 1 C), 107.5 (s, 1 C), 67.0 (s, 4 C), 43.7 (s, 4 C); **ESI-HRMS** (*m/z*): $[M + H]^+$ calc. for $C_{16}H_{22}N_7O_2$, 344.1829; found: 344.1832; **HPLC**: t_R = 8.59 min (96.2% purity).

5-(4,6-Dimorpholino-1,3,5-triazin-2-yl)pyrimidin-2-amine (11) was prepared according to general procedure 2 from 4,4'-(6-chloro-1,3,5-triazine-2,4-diyl)dimorpholine (**7**, 50.0 mg, 170 µmol, 1.0 eq.) and 2-aminopyrimidine-5-boronic acid pinacol ester (155 mg, 700 µmol, 4.0 eq.). Purification by column chromatography on silica gel (ethyl acetate / methanol 1:0 → 20:1) gave compound **11** as a colorless solid (10.0 mg, 29.0 µmol, 17%). **^{1}H NMR** (400 MHz, $(CD_3)_2SO$): δ 9.05 (s, 2 H), 7.26 (br s, 2 H), 3.94-3.62 (m, 8 H), 3.64 (br s, 8 H); **^{13}C{^{1}H} NMR** (101 MHz, $(CD_3)_2SO$): δ 167.2 (s, 1 C), 164.8 (s, 1 C), 164.2 (s, 2 C), 158.6 (s, 2 C), 118.5 (s, 1 C), 66.0 (s, 4 C), 43.2 (br s, 4 C); **ESI-HRMS** (*m/z*): $[M + H]^+$ calc. for $C_{15}H_{21}N_8O_2$, 345.1782; found: 345.1784; **HPLC**: t_R = 6.06 min (95.4% purity).

5-(4,6-Dimorpholino-1,3,5-triazin-2-yl)pyrazin-2-amine (12). 4,4'-(6-iodo-1,3,5-triazine-2,4-diyl)dimorpholine (**8**, 200 mg, 530 µmol, 1.0 eq.), 5-aminopyrazin-2-yl-boronic acid pinacol ester (350 mg, 1.58 mmol, 3.0 eq.), potassium phosphate tribasic (339 mg, 1.60 mmol, 3.0 eq.) and chloro(2-dicyclohexylphosphino-2',4',6'-triisopropyl-1,1'-biphenyl)[2-(2'-amino-1,1'-biphenyl)]palladium(II) (41.7 mg, 53.0 mmol, 0.10 eq.) were charged in a flask. Under nitrogen atmosphere, 1,4-dioxane (5 ml) and deionized H2O (1.5 ml) were added and the resulting mixture was placed into an oil bath pre-heated and allowed to stir for 2 hours at 95 °C. After completion of the reaction, the mixture was allowed to cool to room temperature. Dichloromethane and a 2 M aqueous NaOH-solution were added. The aqueous layer was separated and extracted with dichloromethane (3 x). The combined organic layers were then dried over anhydrous Na2SO4, filtered and the solvent was evaporated under reduced pressure. The crude product was purified by column chromatography on silica gel (dichloromethane / methanol 1:0 → 9:1) to obtain compound **12** as a colorless solid (20.1 mg,

58.4 µmol, 11%). **^{1}H NMR** (400 MHz, $CDCl_3$): δ 9.08 (br s, 1 H), 8.10 (br s, 1 H), 4.86 (br s, 2 H), 4.08-3.81 (m, 8 H), 3.81-3.71 (m, 8 H); **^{13}C{^{1}H} NMR** (101 MHz, $CDCl_3$): δ 168.8 (s, 1 C), 165.2 (s, 2 C), 155.2 (s, 1 C), 144.5 (s, 1 C), 140.1 (s, 1 C), 131.6 (s, 1 C), 67.0 (s, 4 C), 43.8 (br s, 4 C); **ESI-HRMS** (*m/z*): $[M + H]^+$ calc. for $C_{15}H_{21}N_8O_2$, 345.1782; found: 345.1780; **HPLC**: t_R = 5.37 min (95.2% purity).

5-(4,6-Dimorpholino-1,3,5-triazin-2-yl)-4-methylpyridin-2-amine (13) was prepared according to general procedure 2 from 4,4'-(6-chloro-1,3,5-triazine-2,4-diyl)dimorpholine (**7**, 40.0 mg, 140 µmol, 1.0 eq.) and 2-amino-4-methyl-pyridine-5-boronic acid pinacol ester (132 mg, 560 µmol, 4.0 eq.). Purification by column chromatography on silica gel (ethyl acetate / methanol 1:0 → 10:1) gave product **13** as a colorless solid (13.1 mg, 36.7 µmol, 26%). **^{1}H NMR** (400 MHz, $CDCl_3$): δ 8.78 (s, 1 H), 6.33 (s, 1 H), 4.54 (br s, 2 H), 3.90-3.80 (m, 8 H), 3.77-3.72 (m, 8 H), 2.60 (s, 3 H); **^{13}C{^{1}H} NMR** (101 MHz, $CDCl_3$): δ 171.4 (s, 1 C), 165.0 (s, 2 C), 159.3 (s, 1 C), 151.4 (s, 1 C), 149.4 (s, 1 C), 124.1 (s, 1 C), 109.8 (s, 1 C), 66.8 (s, 4 C), 43.7 (br s, 4 C), 22.3 (s, 1 C); **ESI-HRMS** (*m/z*): $[M + H]^+$ calc. for $C_{17}H_{24}N_7O_2$, 358.1986; found: 358.1983; **HPLC**: t_R = 6.57 min (98.5% purity).

5-(4,6-Dimorpholino-1,3,5-triazin-2-yl)-3-methylpyridin-2-amine (14) was prepared according to general procedure 1 from 4,4'-(6-chloro-1,3,5-triazine-2,4-diyl)dimorpholine (**7**, 150 mg, 525 µmol, 1.0 eq.) and boronic acid pinacol ester **23** (180 mg, 622 µmol, 1.2 eq.). Purification by column chromatography on silica gel (cyclohexane / ethyl acetate 1:0 → 4:1) gave product **14** as a colorless solid (116 mg, 32.5 µmol, 62%). **^{1}H NMR** (400 MHz, $CDCl_3$): δ 8.89 (d, $^4J_{H,H}$ = 2.2 Hz, 1 H), 8.22 (br s, 1 H), 5.25 (br s, 2 H), 4.02-3.68 (m, 16 H), 2.19 (s, 3 H); **^{13}C{^{1}H} NMR** (101 MHz, $CDCl_3$): δ 168.9 (s, 1 C), 165.0 (s, 2 C), 158.9 (s, 1 C), 145.2 (s, 1 C), 138.1 (s, 1 C), 123.5 (s, 1 C), 116.3 (s, 1 C), 67.0 (s, 4 C), 43.7 (br s, 4 C), 17.0 (s, 1 C); **ESI-HRMS** (*m/z*): $[M + H]^+$ calc. for $C_{17}H_{24}N_7O_2$, 358.1986; found: 358.1981; **HPLC**: t_R = 6.91 min (99.3% purity).

5-(4,6-Dimorpholino-1,3,5-triazin-2-yl)-3-(trifluoromethyl)pyridin-2-amine (15) was prepared according to general procedure 1 from 4,4'-(6-chloro-1,3,5-triazine-2,4-diyl)dimorpholine (**7**, 83.3 mg, 292 µmol, 1.0 eq.) and boronic acid pinacol ester **24** (100 mg, 292 µmol, 1.0 eq.). Purification by column chromatography on silica gel (cyclohexane / ethyl acetate 1:0 → 1:1) gave product **15** as a colorless solid (89.5 mg, 218 µmol, 75%). **^{1}H NMR** (400 MHz, $CDCl_3$): δ 9.19 (s, 1 H), 8.63 (d, $^4J_{H,F}$ = 2.2 Hz, 1 H), 5.24 (br s, 2 H), 4.01-3.80 (m, 8 H),

3.80-3.71 (m, 8 H); **^{19}F{^{1}H} NMR** (376 MHz, $(CD_3)_2SO$): δ − 63.1 (s, 3 F); **^{13}C{^{1}H} NMR** (101 MHz, $(CD_3)_2SO$): δ 167.3 (s, 1 C), 164.2 (s, 2 C), 157.3 (s, 1 C), 153.1 (s, 1 C), 134.5 (br s, 1 C), 124.1 (q, $^{1}J_{C,F}$ = 271 Hz, 1 C), 119.9 (s, 1 C), 105.1 (q, $^{2}J_{C,F}$ = 31 Hz, 1 C), 66.0 (s, 4 C), 43.2 (br s, 4 C); **ESI-HRMS** (*m/z*): $[M + H]^+$ calc. for $C_{17}H_{21}F_3N_7O_2$, 412.1703; found: 412.1703; **HPLC**: t_R = 8.40 min (> 99.9% purity).

5-(4,6-Dimorpholino-1,3,5-triazin-2-yl)-4-methylpyrimidin-2-amine (16) was prepared according to general procedure 2 from 4,4'-(6-chloro-1,3,5-triazine-2,4-diyl)dimorpholine (**7**, 40.0 mg, 140 µmol, 1.0 eq.) and 4-methyl-5-(4,4,5,5-tetramethyl-1,3,2-dioxaborolan-2-yl)pyrimidin-2-amine (132 mg, 560 µmol, 4.0 eq.). Purification by column chromatography on silica gel (ethyl acetate 100%) gave product **16** as a colorless solid (17.6 mg, 49.2 µmol, 34%). **^{1}H NMR** (400 MHz, $(CD_3)_2SO$): δ 8.90 (s, 1 H), 7.02 (br s, 2 H), 3.81-3.69 (m, 8 H), 3.66-3.59 (m, 8 H), 2.63 (s, 3 H); **^{13}C{^{1}H} NMR** (101 MHz, $CDCl_3$): δ 170.1 (s, 1 C), 168.9 (s, 1 C), 164.6 (s, 2 C), 162.6 (s, 1 C), 160.9 (s, 1 C), 121.3 (s, 1 C), 66.9 (s, 4 C), 43.7 (br s, 4 C), 25.2 (s, 1 C); **ESI-HRMS** (*m/z*): $[M + H]^+$ calc. for $C_{16}H_{23}N_8O_2$, 359.1938; found: 359.1939; **HPLC**: t_R = 6.22 min (97.3% purity).

***N*-(5-(4,6-Dimorpholino-1,3,5-triazin-2-yl)-4-(trifluoromethyl)pyridin-2-yl)acetamide (17).** 5-(4,6-Dimorpholino-1,3,5-triazin-2-yl)-4-(trifluoromethyl)pyridin-2-amine (**1**, 200 mg, 480 µmol, 1.0 eq.) and K_2CO_3 (134 mg, 972 mmol, 2.0 eq.) were mixed in dichloromethane (4 ml) and stirred at room temperature for 5 minutes. Then, the reaction mixture was cooled to 0 °C and acetyl chloride (41.4 µl, 583 mmol, 1.2 eq.) was added dropwise. The resulting mixture was stirred for 3.5 hours and allowed to warm up to room temperature. Then, deionized H_2O was added, the layers were separated and the aqueous layer was extracted with dichloromethane (3 x). The combined organic layers were dried over anhydrous Na_2SO_4, filtered and the solvent was evaporated under reduced pressure. The crude product was purified by column chromatography on silica gel (cyclohexane / ethyl acetate 1:1 → 1:3) to afford compound **17** (120 mg, 265 mmol, 60%) as a colorless solid. **^{1}H NMR** (400 MHz, $CDCl_3$): δ 8.81 (s, 1 H), 8.61 (s, 1 H), 8.34 (s, 1 H), 3.85 (br s, 8 H), 3.78-3.67 (m, 8 H), 2.26 (s, 3 H); **^{19}F{^{1}H} NMR** (376 MHz, $CDCl_3$): δ − 59.5 (s, 3 F); **^{13}C{^{1}H} NMR** (101 MHz, $CDCl_3$): δ 169.3 (s, 1 C), 168.7 (s, 1 C), 164.5 (s, 2 C), 152.6 (s, 1 C), 151.0 (s, 1 C), 138.8 (q, $^{2}J_{C,F}$ = 33 Hz, 1 C), 128.4 (s, 1 C), 122.5 (q, $^{1}J_{C,F}$ = 275 Hz, 1 C), 110.5 (q, $^{3}J_{C,F}$ = 5.1 Hz, 1 C), 66.7 (s, 4 C), 43.5 (br s, 4 C), 24.7 (s, 1 C); **ESI-HRMS** (*m/z*): $[M + H]^+$ calc. for $C_{19}H_{23}F_3N_7O_3$, 454.1809; found: 454.1797; **HPLC**: t_R = 7.94 min (> 99.9% purity).

5-(4,6-dimorpholino-1,3,5-triazin-2-yl)-4-(trifluoromethyl)pyridin-2-ol (18) and **4,4'-(6-(6-Chloro-4-(trifluoromethyl)pyridin-3-yl)-1,3,5-triazine-2,4-diyl)dimorpholine (19).** To a conc. HCl-solution (36%, 5.12 ml) at 0 °C, 5-(4,6-dimorpholino-1,3,5-triazin-2-yl)-4-(trifluoromethyl)pyridin-2-amine (**1**, 500 mg, 1.21 mmol, 1.0 eq.) was added dropwise followed by $NaNO_2$ (1.70 g, 24.6 mmol, 20 eq.). The resulting mixture was then allowed to warm to room temperature over 1 hour and CuCl (4.10 g, 41.4 mmol, 34 eq.) was added. After 1 hour, the reaction mixture was quenched with a 2 M aqueous NaOH-solution and extracted with ethyl acetate (3 x). The combined organic layers were dried over anhydrous Na_2SO_4, filtered and the solvent was evaporated under reduced pressure. The products were separated by column chromatography on silica gel (cyclohexane / ethyl acetate 1:0 → 1:1). Compound **19** (247 mg, 573 µmol, 47%) and compound **18** (166 mg, 403 µmol, 33%) were obtained in two separate fractions and isolated as colorless solids. Compound **19**: **^{1}H NMR** (400 MHz, $CDCl_3$): δ 8.91 (s, 1 H), 7.66 (s, 1 H), 3.89-3.78 (m, 8 H), 3.78-3.68 (m, 8 H); **^{19}F{^{1}H} NMR** (376 MHz, $CDCl_3$): δ − 59.7 (s, 3 F); **^{13}C{^{1}H} NMR** (101 MHz, $CDCl_3$): δ 169.0 (s, 1 C), 164.6 (s, 2 C), 153.2 (s, 1 C), 153.0 (s, 1 C), 154.1 (q, $^2J_{C,F}$ = 34 Hz, 1 C), 131.5 (s, 1 C), 122.1 (q, $^1J_{C,F}$ = 275 Hz, 1 C), 121.4 (q, $^3J_{C,F}$ = 5.4 Hz, 1 C), 66.9 (s, 4 C), 43.8 (br s, 4 C); **ESI-HRMS** (*m/z*): $[M + H]^+$ calc. for $C_{17}H_{19}F_3ClN_6O_2$, 431.1205; found: 431.1199; **HPLC**: t_R = 9.91 min (> 99.9% purity). Compound **18**: **^{1}H NMR** (400 MHz, $(CD_3)_2SO$): δ 12.6 (br s, 1 H), 8.15 (s, 1 H), 6.80 (s, 1 H), 3.79-3.67 (m, 8 H), 3.66-3.55 (m, 8 H); **^{19}F{^{1}H} NMR** (376 MHz, $(CD_3)_2SO$): δ − 59.4 (s, 3 F); **^{13}C{^{1}H} NMR** (101 MHz, $(CD_3)_2SO$): δ 168.0 (s, 1 C), 164.0 (s, 2 C), 161.2 (s, 1 C), 141.4 (br s, 1 C), 138.9 (q, $^2J_{C,F}$ = 32 Hz, 1 C), 122.3 (q, $^1J_{C,F}$ = 275 Hz, 1 C), 119.2 (br s, 1 C), 113.3 (br s, 1 C), 65.9 (s, 4 C), 43.2 (s, 4 C); **ESI-HRMS** (*m/z*): $[M + H]^+$ calc. for $C_{17}H_{20}F_3N_6O_3$, 413.1543; found: 413.1535; **HPLC**: t_R = 6.79 min (99.6% purity).

***N*-(5-(4,6-Dimorpholino-1,3,5-triazin-2-yl)-4-(trifluoromethyl)pyridin-2-yl)-*O*-methylhydroxylamine (20).** 4,4'-(6-(6-Chloro-4-(trifluoromethyl)pyridin-3-yl)-1,3,5-triazine-2,4-diyl)dimorpholine (**19**, 200 mg, 464 µmol, 1.0 eq.), methoxyamine hydrochloride (77.5 mg, 928 µmol, 2.0 eq.) and $NaHCO_3$ (79.0 mg, 940 µmol, 2.0 eq.) were mixed in dimethyl sulfoxide (3.0 ml). The resulting reaction mixture was stirred at 100 °C for 6 hours. The solvent was partially evaporated under reduced pressure. Then, deionized H_2O and dichloromethane were added. The aqueous layer was separated and extracted with dichloromethane (3 x). The combined organic layers were dried over anhydrous Na_2SO_4, filtered and the solvent was evaporated to dryness under reduced pressure. The crude product was purified by column chromatography on silica gel (cyclohexane / ethyl acetate 1:1 → 0:1) to

afford compound **20** (30.0 mg, 34.0 mmol, 15%) as a colorless solid. **^{1}H NMR** (400 MHz, $CDCl_3$): δ 8.77 (s, 1 H), 7.77 (br s, 1 H), 7.23 (s, 1 H), 3.90-3.79 (m, 11 H), 3.77-3.70 (m, 8 H); **^{19}F{^{1}H} NMR** (376 MHz, $CDCl_3$): δ − 59.6 (s, 3 F); **^{13}C{^{1}H} NMR** (101 MHz, $CDCl_3$): δ 169.6 (s, 1 C), 164.8 (s, 2 C), 156.0 (s, 1 C), 151.8 (s, 1 C), 138.6 (q, $^{2}J_{C,F}$ = 274 Hz, 1 C), 127.5 (s, 1 C), 122.6 (q, $^{1}J_{C,F}$ = 275 Hz, 1 C), 110.1 (q, $^{3}J_{C,F}$ = 6.2 Hz, 1 C), 66.9 (s, 4 C), 63.1 (s, 1 C), 43.8 (br s, 4 C); **ESI-HRMS** (*m/z*): $[M + H]^+$ calc. for $C_{18}H_{23}F_3N_7O_3$, 442.1809; found: 442.1799; **HPLC**: t_R = 8.33 min (98.9% purity).

4,4'-(6-(6-Bromo-4-(trifluoromethyl)pyridin-3-yl)-1,3,5-triazine-2,4-diyl)dimorpholine (21).

Compound **1** (1.00 g, 2.43 mmol, 1.0 eq.) was dissolved in dibromomethane (10 ml) and isopentyl nitrite (392 µl, 2.92 mmol, 1.2 eq.) was added. After 5 minutes, a solution of bromotrimethylsilane (401 µl, 3.04 mmol, 1.3 eq.) in dibromomethane (1.5 ml) was added and the resulting reaction mixture was allowed to stir at room temperature for 1 hour. After this time, an aqueous saturated $NaHCO_3$-solution was added, the layers were separated and the aqueous layer was extracted with dichloromethane (3 x). The combined organic layers were dried over anhydrous Na_2SO_4, filtered and the solvent was evaporated under reduced pressure. Purification by column chromatography on silica gel (cyclohexane / ethyl acetate 1:0 → 1:1) gave compound **21** (909 mg, 1.91 mmol, 79% yield) as colorless solid. **^{1}H NMR** (400 MHz, $CDCl_3$): δ 8.88 (s, 1 H), 7.81 (s, 1 H), 3.88-3.78 (m, 8 H), 3.78-3.68 (m, 8 H); **^{19}F{^{1}H} NMR** (376 MHz, $CDCl_3$): δ − 59.6 (s, 3 F); **^{13}C{^{1}H} NMR** (101 MHz, $CDCl_3$): δ 169.0 (s, 1 C), 164.6 (s, 2 C), 153.2 (s, 1 C), 143.7 (s, 1 C), 138.5 (q, $^{2}J_{C,F}$ = 34 Hz, 1 C), 131.8-131.7 (m, 1 C), 125.1 (q, $^{3}J_{C,F}$ = 5.3 Hz, 1 C), 122.0 (q, $^{1}J_{C,F}$ = 275 Hz, 1 C); 66.8 (s, 4 C), 43.7 (br s, 4 C); **ESI-HRMS** (*m/z*): $[M + H]^+$ calc. for $C_{17}H_{19}BrF_3N_6O_2$, 475.0699; found: 475.0710; **HPLC**: t_R = 10.11 min (97.8% purity).

***tert*-Butyl (4-(4,4,5,5-tetramethyl-1,3,2-dioxaborolan-2-yl)phenyl)carbamate (22)** was prepared according to the literature.[33]

***N*,*N*-Dimethyl-*N'*-(3-methyl-5-(4,4,5,5-tetramethyl-1,3,2-dioxaborolan-2-yl)pyridin-2-yl)formimidamide (23)** was prepared according to general procedure 3 from 3-methyl-5-(4,4,5,5-tetramethyl-1,3,2-dioxaborolan-2-yl)pyridin-2-amine (200 mg, 854 µmol, 1.0 eq.). The desired product **23** was obtained in quantitative yield as a brownish solid and was used in the next step without further purification.

^{1}H NMR (400 MHz, $(CD_3)_2SO$): δ 8.50 (s, 1 H), 8.25 (s, 1 H), 7.61 (s, 1 H), 3.10 (s, 3 H), 3.02 (s, 3 H), 2.19 (s, 3 H), 1.27 (s, 12 H).

***N*,*N*-Dimethyl-*N′*-(5-(4,4,5,5-tetramethyl-1,3,2-dioxaborolan-2-yl)-3-(trifluoromethyl)pyridin-2-yl)formimidamide (24)** was prepared according to general procedure 3 from 5-(4,4,5,5-tetramethyl-1,3,2-dioxaborolan-2-yl)-3-(trifluoromethyl)pyridin-2-amine (300 mg, 1.04 mmol, 1.0eq.). The desired product **24** was obtained in quantitative yield as a yellowish solid and was used in the next step without further purification. **^{1}H NMR** (400 MHz, $(CD_3)_2SO$): δ 8.70 (s, 1 H), 8.54 (d, J = 1.8 Hz, 1 H), 7.96 (d, J = 1.9 Hz, 1 H), 3.16 (s, 3 H), 3.06 (s, 3 H), 1.29 (s, 12 H); **^{19}F{^{1}H} NMR** (376 MHz, $(CD_3)_2SO$): δ − 61.6 (s, 3 F).

Protein production and purification.

The ΔABDp110γ was expressed in Sf9 cells using a baculovirus expression system as has been described previously.[24,35] Briefly, human ΔABDp110γ was expressed with a C-terminal His_6-tag and purified by immobilized metal-affinity chromatography, heparin chromatography and gel filtration. The protein in gel filtration buffer (20 mM Tris-HCl 0.5 mM $(NH_4)_2SO_4$, 5 mM DTT, 1% ethylene glycol and 0.02% CHAPS) was concentrated to 8 mg/ml then frozen in liquid nitrogen and stored at -80 °C.

Crystallization of PI3Kγ; soaking with compound 1.

Drops containing 1 µl of ΔABDp110γ protein at 4 mg/ml was and 1 µl of crystallization buffer (16% PEG4K, 250 mM $(NH_4)_2SO_4$, 0.1 M Tris-HCl pH 7.5 at RT) were hair seeded with crushed ΔABDp110γ crystals and incubated at 17°C. The crystals reached their maximum size (0.2 mm × ·0.1mm × 0.1mm) in about 10 days. The inhibitor **1** was prepared in DMSO and diluted in cryo-protectant containing 25% PEG 4000, 15% glycerol, 250mM $(NH_4)_2SO_4$ and 100mM Tris pH 7.5 to a final concentration of 1 mM. The inhibitor in cryo-protectant solution was added to the drop containing the crystals in a stepwise manner. The crystals were soaked in the final 1 mM inhibitor solution for 4 hours. Crystals were then transferred to fresh inhibitor in cryo-protectant solution for 30 s and flash frozen in liquid nitrogen.

Data collection and structure determination.

Diffraction datasets were collected at the ESRF beamline ID23-1 on an ADSC Quantum Q315r detector, using 1.00720 Å wavelength radiation. Images were processed using Mosflm[36] or XDS[37] and scaled

with SCALA[38]. The crystal structure of the ΔABDp110γ/compound **1** complex was solved by molecular replacement using Phaser,[39] with the previously published human ΔABDp110γ as the search model (PDB entry 1E8Y). Coot was used to manually build inhibitors in the unaccounted Fo-Fc difference electron density within the active site of the map.[40] Initial models of the inhibitors were generated from SMILES strings using the ELBOW module of PHENIX.[41] Refmac refinement[42] was iterated with manual rebuilding using Coot until the structure converged. In the final model for the ΔABDp110γ/compound **1** complex, 89.2% of residues were in the core regions of the Ramachandran plot, with one residue in a disallowed region.

Cellular PI3K and mTOR signaling

Downstream signals of PI3K and mTOR were determined in In-Cell Western assays detecting phosphorylation of Ser473 of PKB/Akt (pPKB/Akt) and Ser235/236 on the ribosomal protein S6 (pS6), respectively. Briefly, $2x10^4$ A2058 cells/well in 96-well plates (Cell Carrier, Perkin Elmer) were grown for 24 h, before inhibitors or DMSO were added (1 h; 37°C, 5%CO_2). Cells were subsequently fixed (4% PFA in PBS for 30 min at RT), and then blocked (1% BSA/0.1% Triton X-100/5% goat serum in PBS for 30 min, RT). pPKB/Akt was detected with a rabbit polyclonal antibody (Cell Signaling Technology, #4058), and pS6 with a rabbit monoclonal antibody (Cell Signaling Technology, #4856). Tubulin staining (mouse anti-α-tubulin, Sigma #T9026) was assessed as internal standard. As readout, IRDye680-conjugated goat anti-mouse, and IRDye800-conjugated goat anti-rabbit antibodies (LICOR # 926-68070 and # 926-32211) were used, and fluorescence was measured on an Odyssey CLx infrared imaging scanner (LICOR). Percentage of remaining phospho-substrate signals were calculated in relation to cellular tubulin. Further details and calculations are explained in Ref. 11.

Determination of inhibitor dissociation constants

Dissociation constants of compounds (K_i) for p110α and mTOR were determined by LanthaScreen technology (Life Technologies) as described in detail in [11]. Briefly, the AlexaFluor647-labeled Kinase Tracer314 (#PV6087) was used for p110α with a determined K_d of 2.2 nM at 20 nM, and for mTOR with a K_d of 19 nM used at a final concentration of 10 nM. While recombinant p110α was N-terminally $(His)_6$-tagged, and combined with a biotinylated anti-$(His)_6$-tag antibody (2 nM, #PV6089) and LanthaScreen Eu-Steptavidin (2 nM, #PV5899); truncated mTOR (amino acids 1360-2549; #PR8683B) fused to the C-terminus of GST was detected with a LanthaScreen Eu-labelled anti-GST antibody (2 nM, #PV5594). The p110α assay buffer was composed of 50 mM HEPES pH 7.5, 10 mM $MgCl_2$, 1 mM EGTA, and 0.01% (v/v) Brij-35, and the mTOR assay buffer

contained 50 mM HEPES; 5 mM $MgCl_2$; 1mM EGTA; 0.01% Pluronic F-127. Further details and calculations are described in Ref. 11.

Cell cycle analysis.

A2058 cells (1-2 $x10^5$ cells/ml) or SKOV3 cells (0.25- 0.5 $x10^5$ cells/ml) were seeded in DMEM supplemented with 10% heat-inactivated FCS, 1% L-glutamine, and 1% penicillin-streptomycin (2 ml/ well of 6-well plates. The day after, inhibitors (5 μM for A2058, 2 μM for SKOV3) were added for 24h. Subsequently non-adherent cells were collected by centrifugation, adherent cells were detached, fixed and permeabilized - combined with the previously non-adherent cell - in PBS supplemented with 4% paraformaldehyde/ 1% bovine serum albumin/0.1% TritonX-100 for 30 min. at 4°C then washed with 1% bovine serum albumin/0.1% TritonX-100 in PBS followed by DNA-staining with 50 μg/ml propidium iodide in 0.1% TritonX-100/0.1% sodium citrate solution (pH 7.4) containing 10 μg/ml DNase-free RNase (>1h , RT, in the dark). Cell cycle profiles were acquired by fluorescence activated cell sorting (FACSCanto II, Becton Dickinson) and analyzed with FlowJo (Treestar) software.

Western blotting.

Cells were lysed in NP40-based lysis buffer (20 mM Tris-HCl pH 8, 138 mM NaCl, 2.7 mM KCl, 5% glycerol, 1% NP-40) supplemented with protease and phosphatase inhibitors, cleared by centrifugation and denatured by adding 5x sample buffer and boiling at 96°C for 6 min. Equal amount of proteins were subjected to SDS-PAGE and transferred to Immobilon FL membranes (Millipore). Primary antibodies to pSer473-PKB/Akt (#4058L), pThr308-PKB/Akt (#4056L), PKB/AKT (#2929S), pT389-S6K1 (#9206S), pS235/236 ribosomal protein S6 (#4856S); S6K1 (#9202S) and ribosomal protein S6 (#2317S) were from Cell Signaling Technology; and primary antibody to α-tubulin (#T9026) was from Sigma. HRP-conjugated secondary antibodies were visualized using enhanced chemiluminescence (Millipore) on a Fusion FX (Vilber Lourmat) imaging system. Levels of phosphorylated proteins were quantified using ImageJ and normalized to their respective non-phosphorylated proteins.

Kinome profiling.

The inhibitory capacity and selectivity of compound was determined using the ScanMax platform provided by DiscoverX.[26] In short binding of immobilized ligand to DNA-tagged kinases was competed with 10μM compound. The amount of kinase bound to the immobilized ligand was measured by quantitative PCR of

the respective DNA tags and is given as percentage of control. Binding constants of compounds for kinases of interest were determined by competing the immobilized ligand kinase interactions with an 11-point 3-fold serial dilution of compound starting from 30 μM and subsequent quantitative PCR of DNA tags. Binding constants were calculated by a standard dose-response curve using the Hill equation:

Response = Background + (Signal - Background)/(1 + 10^([lg Kd - lg dose] * HillSlope)); with Hill Slope set to -1.

Cell proliferation assay panels.

NCI60: Detailed procedures on compound and cell handling are available from https://dtp.cancer.gov/discovery_development/nci-60/methodology.htm. Briefly, human tumor cell lines were seeded into 96 well microtiter plates, and exposed to 5 (½ log serial) drug dilutions plus control, followed by 48 h (except for two controls of each cell line which were fixed with TCA (cell population at t = 0 h [Tz]). The assay was terminated by fixation with TCA (10% final). Cell density was determined using a Sulforhodamine B staining protocol and the absorbance measured at 515 nm. Using seven absorbance measurements [Tz; control growth (C); growth with drugs added (Ti)], the percentage growth was calculated at each of the drug concentrations levels. Percentage growth inhibition is calculated as:

[(Ti-Tz)/(C-Tz)] x 100 for concentrations for which Ti≥Tz; and

[(Ti-Tz)/Tz] x 100 for concentrations for which Ti<Tz

The NTRC Oncolines 44 cell lines were exposed for 72 h to 9-point 3-fold serial dilutions of **1** as described in Ref. 11. The concentration of 50% growth inhibition is associated with the signal: $((luminescence_{\text{untreated,t=72h}} - luminescence_{t=0})/2) + luminescence_{t=0}$. The dataset integrated here was used for IC_{50} calculations in Ref. 11.

IC_{50}s of A2058 or SKOV3 cell proliferation given in Table 2 were determined and calculated as described in Ref. 11 for the indicated compounds.

PC3 xenograft model in nude rats.

Compound Preparation and Dosing: Compound **1** was dissolved in DMSO to 40 mg/ml. This solution was diluted with 20% HPBCD [(2-Hydroxypropyl)-β-cyclodextrin, in water for injection (Lavoisier, batch #2F274 5) in order to reach a final concentration of **1** of 4 mg/ml. Successive dilutions in vehicle (DMSO/20%

HPBCD solution, 10/90, v/v) were performed to reach 1, 2 and 3 mg/ml final concentrations. Vinorelbine was diluted in 0.9% NaCl solution to 0.5 mg/ml. Treatment doses for **1** were 5, 10 and 15 mg/kg, and 2.5 mg/kg for Vinorelbine. Rats were given compound **1** by oral gavage (p.o.), Vinorelbine intravenously (i.v., as bolus) into the tail vain. The p.o. administration volume and the IV injection volume were 5 ml/kg.

Animals and animal handling: healthy male nude NIH rats (Crl:NIH-Foxn1 rnu, Charles River, Germany) bread in a specific-pathogen-free (SPF) animal care unit were fed sterile, irradiated food granules (V1246-703, Soest, Germany). Animal procedures were reviewed by the Animal Care and Use Committee of Pharmacy and Medicine University of Dijon or Oncodesign's ethical committee.

Cell culture: PC-3 prostatic adenocarcinoma tumor cells (ATCC, CRL-1435) were grown as monolayer in complete RPMI1640 medium, supplemented with 10% FBS (37°C, 5% CO_2). Tumor cells were detached with trypsin-Versene (Lonza; 5 min in in Hanks' medium without Ca^{2+} or Mg^{2+}, then resuspended in complete RPMI1640.

Tumor model: $2x10^7$ PC-3 cells were injected subcutaneously at day 0 (D0) in 200 µl RPMI1640 into the right flank of male nude rats, 24 hours after a whole-body irradiation with a γ-source (5 Gy, ^{60}Co). Tumor-bearing rats were randomized on day 16 (mean volume of 330 ± 70 mm^3 according to their individual tumor volume into 5 groups of each 8 animals using Vivo manager® software (Bio-systemes, Couternon, France). Analysis of variance was performed to test for homogeneity between groups.

Treatment schedule: Daily administration on D17 to D44 and from D51 to D57: *Group 1*: vehicle; *Group 2*: compound **1** at 5 mg/kg; *Group 3*: **1** at 10 mg/kg. *Group 4*: **1** at 15 mg/kg from D17 to D21, from D24 to D28, from D34 to D38, from D41 to D45 and from D51 to D56. Group 5: one IV injection of Vinorelbine at 2.5 mg/kg on D17, D24, D31 and D38. Final termination of rats was performed on D87.

Body weight was measured at least twice a week. Length and width of tumors were measured and recorded twice a week with calipers and the tumor volume was estimated by the formula:

$$\text{Tumor volume} = ½ * \text{length} * (\text{width})^2$$

Glucose and insulin levels determination: Glucose was measured using kit CBA086 from Calbiochem; insulin was determined using kit EZRMI-13K from EMD Millipore, according to the manufacturer's instructions.

PK/PD studies in nude rat PC3 xenograft model

*Pharmacokinetic study of compound **1** in PC-3 tumor bearing rats:* Induction of PC-3 subcutaneous

tumors is described above. Animals were randomized on D21 when the tumors reached 575 ± 267 mm^3 (D20). 27 animals were randomized according to their individual tumor volume into 3 groups (one group of 3 rats and two groups of 12 rats) using Vivo manager® software (Biosystemes, Couternon, France).

Treatment Q1Dx1 - *Group 1*: 3 rats single i.v. injection of vehicle. *Group 2*: 12 and 3 satellite rats single i.v. injection of **1** (10.3 mg/kg). *Group 3*: 12 and 3 satellite rats single p.o. administration of compound **1** (16.55 mg/kg). On selected time points blood, brain, liver and tumor from 3 rats from each group were collected to determine levels of **1**, glucose and insulin, or analyze pPKB/Akt in tissues.

Solubility assays.

Stock solutions of compounds were prepared in DMSO at 20 mM. From these, 200 µM solutions were made up by a direct dilution of the stock solution with a phosphate buffer (PBS, pH 7.4) or citrate buffer (pH 4.0). Reference solutions were made up in 100% MeOH. Solutions in buffer (200 µl) were incubated and agitated at room temperature for 1 hr, and then centrifuged at 13000 rpm for 10 minutes. A volume of 100 µl of the supernatants were diluted with 100 µl of MeOH:PBS:Citrate 8:1:1 and analyzed by LC/MS.

Structure modelling of compound 1/mTOR kinase complexes.

The coordinates of mTOR kinase 4JT6 (3.6 Å) and 4JSN (3.2 Å) were used as starting points to dock **1** into the ATP-binding site of mTOR kinase. Docking of the ligand **1** to mTOR was performed using SwissDock (swissdock.ch), and energy minimization was performed using YASARA's default settings. Alternatively, the PI103 ligand in 4JT6 was manually replaced by **1** docking one of its morpholino groups to Val2240, before energy minimizations were performed. The docking procedures were validated by redocking **1** into the apoprotein of the **1**/PI3Kγ complex (PDB ID 5OQ4).

ASSOCIATED CONTENT

Supporting Information

Supporting information is available via the Internet at http://pubs.acs.org

X-Ray crystallography parameters and refinement values for **1** (Table S1, page 3); a TREEspot representation (Figure S1, page 4) and its raw data (Table S2, pages 5-16); the anti-proliferative action of compound **1** in four cell line panels (Table S3, pages 17-19); extended Tables S4 (page 20) and S5 (page 21) with in vitro pharmacology data; the safety profile of **1** (Table S6, page 22); the comparative solubility of **1** (Table S7, page 23); the efficacy of compound **1** intermittent dosing in tumor bearing rats (Figure S2, page 24); ^{1}H-NMR spectra (pages 23-33); ^{19}F{^{1}H} NMR spectra (pages 34-37); ^{13}C{^{1}H} NMR spectra (pages 38-45); ESI-HRMS Spectra (pages 46-52); MALDI-MS Spectra (pages 53); and HPLC Chromatograms (pages 54-60) are added as Supporting Information. An appendix of chemical formula of compounds synthesized here is on page 61.

Accession Codes

The coordinates of compound **1** in PI3Kγ have been deposited with PDB ID code 5OQ4 at wwpdb.org and rcsb.org.

AUTHOR INFORMATION

Corresponding Authors

Phone: +41 61 207 5046. Fax: +41 61 207 3566.

E-mail: Matthias.Wymann@UniBas.CH; Denise.Rageot@unibas.ch

Notes: conflicts of interest

FB, NC, VC, JM, PHe, PHi, and DF are current or past employees of PIQUR Therapeutics AG, Basel; and NC, VC, JM, PHe, PHi, DF, BG and MPW are shareholders of PIQUR Therapeutics AG.

ACKNOWLEGEMENTS

We thank A. Pfaltz, R.A. Ettlin, W. Dieterle, J.-B. Langlois, S. Mukherjee and M. Lang for advice and discussions; S. Bünger and A. Dall Asen for technical assistance; master students of the Department of Chemistry for early synthetic efforts; M. Neuburger and D. Häussinger for chemical structure determination. We are grateful to G. Zaman and the NTRC team for help and expertise with high content screening assays. This work was supported by the Swiss Commission for Technology and Innovation (CTI) by PFLS-LS grants 14032.1, 15811.2, and 17241.1; the Stiftung für Krebsbekämpfung grant 341, Swiss National Science Foundation grants 310030_153211 and 316030_133860 (to MPW), and 310030B_138659; and in part by European Union's Horizon 2020 research and innovation programme under the Marie Skłodowska-Curie grant agreement 675392; and by the MRC to RLW (MC_U105184308).

ABBREVIATIONS USED

DNA-PK DNA-dependent protein kinase

ESI: electrospray ionization

GPCR: G-protein coupled receptor

mTOR: mammalian target of rapamycin

PI3K: phosphoinositide 3-kinase

PKB/Akt: protein kinase B/Akt

PSA: polar surface area

PtdIns(4,5)P_2: phosphatidylinositol(4,5)-bisphosphate

PtdIns(3,4,5)P_3: phosphatidylinositol(3,4,5)-trisphosphate

S6: ribosomal protein S6

S6K: S6 kinase

SH2: src-homology 2

TORC1: mTOR complex 1

VPS34: vacuolar protein sorting 34, the class III PI3K

REFERENCES

(1) Wymann, M. P., Schneiter, R. Lipid signalling in disease. *Nat. Rev. Mol. Cell Biol.* **2008**, *9*, 162-176.

(2) Thorpe, L. M., Yuzugullu, H., Zhao, J. J. PI3K in cancer: divergent roles of isoforms, modes of activation and therapeutic targeting. *Nat. Rev. Cancer* **2015**, *15*, 7-24.

(3) Engelman, J. A. Targeting PI3K signalling in cancer: opportunities, challenges and limitations. *Nat. Rev. Cancer* **2009**, *9*, 550-562.

(4) Wymann, M. PI3Ks-Drug targets in inflammation and cancer. *Subcell. Biochem.* **2012**, *58*, 111-181.

(5) Arteaga, C. L., Sliwkowski, M. X., Osborne, C. K., Perez, E. A., Puglisi, F., Gianni, L. Treatment of HER2-positive breast cancer: current status and future perspectives. *Nat. Rev. Clin. Oncol.* **2012**, *9*, 16-32.

(6) Sun, T., Aceto, N., Meerbrey, K. L., Kessler, J. D., Zhou, C., Migliaccio, I., Nguyen, D. X., Pavlova, N. N., Botero, M., Huang, J., Bernardi, R. J., Schmitt, E., Hu, G., Li, M. Z., Dephoure, N., Gygi, S. P., Rao, M., Creighton, C. J., Hilsenbeck, S. G., Shaw, C. A., Muzny, D., Gibbs, R. A., Wheeler, D. A., Osborne, C. K., Schiff, R., Bentires-Alj, M., Elledge, S. J., Westbrook, T. F. Activation of multiple proto-oncogenic tyrosine kinases in breast cancer via loss of the PTPN12 phosphatase. *Cell* **2011**, *144*, 703-718.

(7) Samuels, Y., Ericson, K. Oncogenic PI3K and its role in cancer. *Curr. Opin. Oncol.* **2006**, *18*, 77-82.

(8) Hollander, M. C., Blumenthal, G. M., Dennis, P. A. PTEN loss in the continuum of common cancers, rare syndromes and mouse models. *Nat. Rev. Cancer* **2011**, *11*, 289-301.

(9) Gewinner, C., Wang, Z. C., Richardson, A., Teruya-Feldstein, J., Etemadmoghadam, D., Bowtell, D., Barretina, J., Lin, W. M., Rameh, L., Salmena, L., Pandolfi, P. P., Cantley, L. C. Evidence that inositol polyphosphate 4-phosphatase type II is a tumor suppressor that inhibits PI3K signaling. *Cancer Cell* **2009**, *16*, 115-125.

(10) (a) Liu, P., Cheng, H., Roberts, T. M., Zhao, J. J. Targeting the phosphoinositide 3-kinase pathway in cancer. *Nat. Rev. Drug Discov.* **2009**, *8*, 627-644.; (b) LoRusso, P. M. Inhibition of the PI3K/AKT/mTOR pathway in solid tumors. *J. Clin. Oncol.* **2016**, *34,* 3803-3815.

(11) Bohnacker, T., Prota, A. E., Beaufils, F., Burke, J. E., Melone, A., Inglis, A. J., Rageot, D., Sele, A. M., Cmiljanovic, V., Cmiljanovic, N., Bargsten, K., Aher, A., Akhmanova, A., Díaz, J. F., Fabbro, D., Zvelebil, M., Williams, R. L., Steinmetz, M. O., Wymann, M. P. Deconvolution of Buparlisib's mechanism of action defines specific PI3K and tubulin inhibitors for therapeutic intervention. *Nat. Commun.* **2017**, *8*, 14683.

(12) (a) Yaguchi, S., Fukui, Y., Koshimizu, I., Yoshimi, H., Matsuno, T., Gouda, H., Hirono, S., Yamazaki, K., Yamori, T. Antitumor activity of ZSTK474, a new phosphatidylinositol 3-kinase inhibitor. *J. Natl. Cancer Inst.* **2006**, *98*, 545-556.; (b) Rewcastle, G. W., Gamage, S. A., Flanagan, J. U., Frederick, R., Denny, W. A., Baguley, B. C., Kestell, P., Singh, R., Kendall, J. D., Marshall, E. S., Lill, C. L., Lee, W. J., Kolekar, S., Buchanan, C. M., Jamieson, S. M., Shepherd, P. R. Synthesis and biological evaluation of novel analogues of the pan class I phosphatidylinositol 3-kinase (PI3K) inhibitor 2-

(difluoromethyl)-1-[4,6-di(4-morpholinyl)-1,3,5-triazin-2-yl]-1H-benzimidazole (ZSTK474). *J. Med. Chem.* **2011**, *54*, 7105-7126.

(13) Brachmann, S. M., Kleylein-Sohn, J., Gaulis, S., Kauffmann, A., Blommers, M. J., Kazic-Legueux, M., Laborde, L., Hattenberger, M., Stauffer, F., Vaxelaire, J., Romanet, V., Henry, C., Murakami, M., Guthy, D., Sterker, D., Bergling, S., Wilson, C., Bruemmendorf, T., Fritsch, C., Garcia-Echeverria, C., Sellers, W. R., Hofmann, F., Maira, S. M. Characterization of the mechanism of action of the pan class I PI3K inhibitor NVP-BKM120 across a broad range of concentrations. *Mol. Cancer Ther.* **2012**, *11*, 1747-1757.

(14) Elkabets, M., Vora, S., Juric, D., Morse, N., Mino-Kenudson, M., Muranen, T., Tao, J., Campos, A. B., Rodon, J., Ibrahim, Y. H., Serra, V., Rodrik-Outmezguine, V., Hazra, S., Singh, S., Kim, P., Quadt, C., Liu, M., Huang, A., Rosen, N., Engelman, J. A., Scaltriti, M., Baselga, J. mTORC1 inhibition is required for sensitivity to PI3K p110alpha inhibitors in PIK3CA-mutant breast cancer. *Sci. Transl. Med.* **2013**, *5*, 196ra99.

(15) Zoncu, R., Efeyan, A., Sabatini, D. M. mTOR: from growth signal integration to cancer, diabetes and ageing. *Nat. Rev. Mol. Cell. Biol.* **2011**, *12*, 21-35.

(16) Marone, R., Cmiljanovic, V., Giese, B., Wymann, M. P. Targeting phosphoinositide 3-kinase: moving towards therapy. *Biochim. Biophys. Acta* **2008**, *1784*, 159-185.

(17) Marone, R., Erhart, D., Mertz, A. C., Bohnacker, T., Schnell, C., Cmiljanovic, V., Stauffer, F., Garcia-Echeverria, C., Giese, B., Maira, S. M., Wymann, M. P. Targeting melanoma with dual phosphoinositide 3-kinase/mammalian target of rapamycin inhibitors. *Mol. Cancer Res.* **2009**, *7*, 601-613.

(18) Corcoran, R. B., Rothenberg, S. M., Hata, A. N., Faber, A. C., Piris, A., Nazarian, R. M., Brown, R. D., Godfrey, J. T., Winokur, D., Walsh, J., Mino-Kenudson, M., Maheswaran, S., Settleman, J., Wargo, J. A., Flaherty, K. T., Haber, D. A., Engelman, J. A. TORC1 suppression predicts responsiveness to RAF and MEK inhibition in BRAF-mutant melanoma. *Sci. Transl. Med.* **2013**, *5*, 196ra98.

(19) Burger, M. T., Pecchi, S., Wagman, A., Ni, Z. J., Knapp, M., Hendrickson, T., Atallah, G., Pfister, K., Zhang, Y., Bartulis, S., Frazier, K., Ng, S., Smith, A., Verhagen, J., Haznedar, J., Huh, K., Iwanowicz, E., Xin, X., Menezes, D., Merritt, H., Lee, I., Wiesmann, M., Kaufman, S., Crawford, K., Chin, M., Bussiere, D., Shoemaker, K., Zaror, I., Maira, S. M., Voliva, C. F. Identification of NVP-BKM120 as a potent, selective, orally bioavailable class I PI3 kinase inhibitor for treating cancer. *ACS Med. Chem. Lett.* **2011**, *2*, 774-779.

(20) Sutherlin, D. P., Bao, L., Berry, M., Castanedo, G., Chuckowree, I., Dotson, J., Folks, A., Friedman, L., Goldsmith, R., Gunzner, J., Heffron, T., Lesnick, J., Lewis, C., Mathieu, S., Murray, J., Nonomiya, J., Pang, J., Pegg, N., Prior, W. W., Rouge, L., Salphati, L., Sampath, D., Tian, Q., Tsui, V., Wan, N. C., Wang, S., Wei, B., Wiesmann, C., Wu, P., Zhu, B. Y., Olivero, A. Discovery of a potent, selective, and orally available class I phosphatidylinositol 3-kinase (PI3K)/mammalian target of rapamycin (mTOR) kinase inhibitor (GDC-0980) for the treatment of cancer. *J. Med. Chem.* **2011**, *54*, 7579-7587.

(21) Dehnhardt, C. M., Venkatesan, A. M., Chen, Z., Delos-Santos, E., Ayral-Kaloustian, S., Brooijmans, N., Yu, K., Hollander, I., Feldberg, L., Lucas, J., Mallon, R. Identification of 2-oxatriazines as highly potent pan-PI3K/mTOR dual inhibitors. *Bioorg. Med. Chem. Lett.* **2011**, *21*, 4773-4778.

(22) Folkes, A. J., Ahmadi, K., Alderton, W. K., Alix, S., Baker, S. J., Box, G., Chuckowree, I. S., Clarke, P. A., Depledge, P., Eccles, S. A., Friedman, L. S., Hayes, A., Hancox, T. C., Kugendradas, A., Lensun, L., Moore, P., Olivero, A. G., Pang, J., Patel, S., Pergl-Wilson, G. H., Raynaud, F. I., Robson, A., Saghir, N., Salphati, L., Sohal, S., Ultsch, M. H., Valenti, M., Wallweber, H. J., Wan, N. C., Wiesmann, C., Workman, P., Zhyvoloup, A., Zvelebil, M. J., Shuttleworth, S. J. The identification of 2-(1H-indazol-4-yl)-6-(4-methanesulfonyl-piperazin-1-ylmethyl)-4-morpholin -4-yl-thieno[3,2-d]pyrimidine (GDC-0941) as a potent, selective, orally bioavailable inhibitor of class I PI3 kinase for the treatment of cancer. *J. Med. Chem.* **2008**, *51,* 5522-5532.

(23) Arcaro, A., Wymann, M. P. Wortmannin is a potent phosphatidylinositol 3-kinase inhibitor: the role of phosphatidylinositol 3,4,5-trisphosphate in neutrophil responses. *Biochem. J.* **1993**, *296*, 297-301.

(24) Wymann, M. P., Bulgarelli-Leva, G., Zvelebil, M. J., Pirola, L., Vanhaesebroeck, B., Waterfield, M. D., Panayotou, G. Wortmannin inactivates phosphoinositide 3-kinase by covalent modification of Lys-802, a residue involved in the phosphate transfer reaction. *Mol. Cell. Biol.* **1996**, *16*, 1722-1733.

(25) Venkatesan, A. M., Dehnhardt, C. M., Delos Santos, E., Chen, Z., Dos Santos, O., Ayral-Kaloustian, S., Khafizova, G., Brooijmans, N., Mallon, R., Hollander, I., Feldberg, L., Lucas, J., Yu, K., Gibbons, J., Abraham, R. T., Chaudhary, I., Mansour, T. S. Bis(morpholino-1,3,5-triazine) derivatives: potent adenosine 5'-triphosphate competitive phosphatidylinositol-3-kinase/mammalian target of rapamycin inhibitors: discovery of compound 26 (PKI-587), a highly efficacious dual inhibitor. *J. Med. Chem.* **2010**, *53*, 2636-2645.

(26) Fabian, M. A., Biggs, W. H., Treiber, D. K., Atteridge, C. E., Azimioara, M. D., Benedetti, M. G., Carter, T. A., Ciceri, P., Edeen, P. T., Floyd, M., Ford, J. M., Galvin, M., Gerlach, J. L., Grotzfeld, R. M., Herrgard, S., Insko, D. E., Insko, M. A., Lai, A. G., Lélias, J. M., Mehta, S. A., Milanov, Z. V., Velasco, A. M., Wodicka, L. M., Patel, H. K., Zarrinkar, P. P., Lockhart, D. J. A small molecule-kinase interaction map for clinical kinase inhibitors. *Nat. Biotechnol.* **2005**, *23*, 329-336.

(27) Zask, A., Verheijen, J. C., Curran, K., Kaplan, J., Richard, D. J., Nowak, P., Malwitz, D. J., Brooijmans, N., Bard, J., Svenson, K., Lucas, J., Toral-Barza, L., Zhang, W. G., Hollander, I., Gibbons, J. J., Abraham, R. T., Ayral-Kaloustian, S., Mansour, T. S., Yu, K. ATP-competitive inhibitors of the mammalian target of rapamycin: design and synthesis of highly potent and selective pyrazolopyrimidines. *J. Med. Chem.* **2009**, *52*, 5013-5016.

(28) Walker, E. H., Pacold, M. E., Perisic, O., Stephens, L., Hawkins, P. T., Wymann, M. P., Williams, R. L. Structural determinants of phosphoinositide 3-kinase inhibition by wortmannin, LY294002, quercetin, myricetin, and staurosporine. *Mol. Cell* **2000**, *6*, 909-919.

(29) O'Reilly, K. E., Rojo, F., She, Q. B., Solit, D., Mills, G. B., Smith, D., Lane, H., Hofmann, F., Hicklin, D. J., Ludwig, D. L., Baselga, J., Rosen, N. mTOR inhibition induces upstream receptor tyrosine kinase signaling and activates Akt. *Cancer Res.* **2006**, *66*, 1500-1508.

(30) Karaman, M. W., Herrgard, S., Treiber, D. K., Gallant, P., Atteridge, C. E., Campbell, B. T., Chan, K. W., Ciceri, P., Davis, M. I., Edeen, P. T., Faraoni, R., Floyd, M., Hunt, J. P., Lockhart, D. J., Milanov, Z. V., Morrison, M. J., Pallares, G., Patel, H. K., Pritchard, S., Wodicka, L. M., Zarrinkar, P. P. A quantitative analysis of kinase inhibitor selectivity. *Nat. Biotechnol.* **2008**, *26*, 127-132.

(31) Shoemaker, R. H. The NCI60 human tumour cell line anticancer drug screen. *Nat. Rev. Cancer* **2006**, *6*, *813-823*.

(32) Pollak, M. The insulin and insulin-like growth factor receptor family in neoplasia: an update. *Nat. Rev. Cancer* **2012**, *12*, 159-169.

(33) Sugino, M., Hatanaka, K., Araki, Y., Hisaki, I., Miyata, M., Tohnai, N. Amphiphilic inclusion spaces for various guests and regulation of fluorescence intensity of 1,8-bis(4-aminophenyl)anthracene crystals. *Chemistry* **2014**, *20*, 3069-3076.

(34) Zhao, X., Tan Q., Zhang Z, Zhao, Y. 1,3,5-Triazine inhibitors of histone deacetylases: synthesis and biological activity. *Med. Chem. Res.* **2014**, *23*, 5188-5196.

(35) Knight, Z. A., Gonzalez, B., Feldman, M. E., Zunder, E. R., Goldenberg, D. D., Williams, O., Loewith, R., Stokoe, D., Balla, A., Toth, B., Balla, T., Weiss, W. A., Williams, R. L., Shokat, K. M. A pharmacological map of the PI3-K family defines a role for p110alpha in insulin signaling. *Cell* **2006**, *125*, 733-747.

(36) Leslie, A. G. W. Mosflm-a programme for processing X-ray diffraction data. *Jnt CCP4/ESF–EACBM Newsl. Protein Crystallogr.* **1992**, No. 26, (Daresbury Laboratory, Warrington, 1992).

(37) Kabsch, W. Automatic processing of rotation diffraction data from crystals of initially unknown symmetry and cell constants. *J. Appl. Crystallogr.* **1993**, *26*, 795-800.

(38) CCP4 The CCP4 suite: programs for protein crystallography. *Acta Crystallogr. D. Biol. Crystallogr.* **1994**, *50*, 760-763.

(39) McCoy, A. J. Solving structures of protein complexes by molecular replacement with Phaser. *Acta Crystallogr. D. Biol. Crystallogr.* **2007**, *63*, 32-41.

(40) Emsley, P., Cowtan, K. Coot: model-building tools for molecular graphics. *Acta Crystallogr. D. Biol. Crystallogr.* **2004**, *60*, 2126-2132.

(41) Moriarty, N. W., Grosse-Kunstleve, R. W., Adams, P. D. Electronic ligand builder and optimization workbench (eLBOW): a tool for ligand coordinate and restraint generation. *Acta Crystallogr. D. Biol. Crystallogr.* **2009**, *65*, 1074-1080.

(42) Murshudov, G. N., Vagin, A. A., Dodson, E. J. Refinement of macromolecular structures by the maximum-likelihood method. *Acta Crystallogr. D. Biol. Crystallogr.* **1997**, *53*, 240-255.

TABLE OF CONTENTS GRAPHIC